S T E L L I N G E N

I

Bij computerberekeningen voor kernreactoren verdient het aanbeveling gebruik te maken van een beeldbuis (display unit) bij het invoeren van gegevens betreffende de geometrie van het rekenmodel.

II

De mate van gebruik van analoge en/of hybride rekenmachines bij het ontwerpen van kernreactoren zal afnemen.

III

De bewering van Wennemo-Hanssen, dat uit een gemeten spectrum index (gedefiniëerd in vergelijking (3.4) van dit proefschrift) energie-gemiddelde werkzame doorsneden kunnen worden afgeleid, is in haar algemeenheid onjuist. Ook Stamm'lers bewering, dat de spectrum index als parameter voor het karakteriseren van het thermische neutronen spectrum geschikter is dan de gemiddelde snelheid van de neutronen, is aanvechtbaar.

S.E. Wennemo-Hanssen, Nucl. Sci. and Eng. 38 (1969) 42.
R.J.J. Stamm'ler, Acad. Proefschrift Delft, Stelling 5 (1968).

IV

Uit het feit dat de verhouding van de absorptie- en de splijtings-werkzame doorsneden van ^{239}Pu in de resonantie bij 0.3 eV toeneemt kan niet zonder meer geconcludeerd worden dat ^{239}Pu een negatieve bijdrage levert aan de temperatuurscoëfficiënt van thermische reactoren.

V

De diagonale transport correctie van de verstrooiingsmatrix van modererende materialen veroorzaakt noch een verharding, noch een verzachting van het neutronen spectrum in een oneindig uitgebreid homogeen medium.

R.J.J. Stamm'ler e.a., "Neutron thermalization in reactor lattice cells: An NPY-Project Report", Technical Reports Series No. 68, IAEA, Vienna (1966).

VI

Gezien het belang van een optimaal reactorontwerp dient in Europa naast industriële research ook onderzoek gedaan te worden in centra waar het leveren van een ontwerp niet aan een tijdslimiet gebonden is.

VII

Het tertiair onderwijs in de reactorkunde in Nederland dient in één instituut geconcentreerd te worden.

VIII

Toename van de individualisering van het basisonderwijs gaat gepaard met een toename van het aantal overspannen leerkrachten.

IX

Bij de liturgievernieuwing in de rooms-katholieke kerk in Nederland zijn onjuiste maatregelen genomen betreffende de veranderingen in de kerkmuziek.

X

De gebruikelijke argumenten voor het al dan niet invoeren van een vereenvoudigde spelling vertonen veel overeenkomst met de argumenten vóór en tegen het klavarscribo notenschrift.

A.J. Janssen

Delft, 9 december 1971

CALCULATION AND MEASUREMENT OF THERMAL NEUTRON SPECTRA IN NON-UNIFORM REACTOR LATTICES

CALCULATION AND MEASUREMENT OF THERMAL NEUTRON SPECTRA IN NON-UNIFORM REACTOR LATTICES

PROEFSCHRIFT
TER VERKRIJGING VAN DE GRAAD VAN DOCTOR IN DE
TECHNISCHE WETENSCHAPPEN AAN DE TECHNISCHE
HOGESCHOOL DELFT, OP GEZAG VAN DE RECTOR
MAGNIFICUS IR. H.R. VAN NAUTA LEMKE,
HOOGLERAAR IN DE AFDELING DER ELEKTROTECHNIEK,
VOOR EEN COMMISSIE UIT DE SENAAT TE
VERDEDIGEN OP DONDERDAG 9 DECEMBER 1971
TE 16 UUR

DOOR

ANTONIUS JOHANNES JANSSEN

NATUURKUNDIG INGENIEUR
GEBOREN TE ENSCHEDE

Druk: Roeland-foto-offset n.v., 's-Gravenhage

DIT PROEFSCHRIFT IS GOEDGEKEURD DOOR DE PROMOTOR

PROF.DR. J.J. WENT.

" Scribenda gerere et gesta scribere "

C O N T E N T S

		page
1.	INTRODUCTION	1
2.	CALCULATION METHODS	6
	2.1 Introduction	6
	2.2 The two-dimensional integral transport equation for linear anisotropic scattering; the THERMOGENE program	7
	2.3 Treatment of arbitrary two-dimensional geometries in THERMOGENE	13
	2.4 Effect of discretization on the accuracy of calculated results	17
	2.5 Calculated results obtained with THERMOGENE	20
3.	EXPERIMENTAL TECHNIQUES	29
	3.1 General considerations	29
	3.2 The time-of-flight spectrometer	30
	3.2.1 Principle	30
	3.2.2 Adaptation of the spectrometer	32
	3.2.3 Analysis of data	34
	3.2.3.1 Calibration of time scale	34
	3.2.3.2 Background	35
	3.2.3.3 Transmission function	36
	3.2.3.4 Detector efficiency	39
	3.2.3.5 Other corrections	41
	3.2.4 Accuracy of the measured spectra	43
	3.3 Activation techniques	44
	3.3.1 General considerations	44
	3.3.2 Analysis of data	44
	3.3.3 Accuracy of the measured activation	49

page

4. COMPARISON BETWEEN CALCULATIONS AND MEASUREMENTS 50

4.1 General considerations 50

4.2 Systems with square rods 55

4.3 Systems with circular rods 61

4.4 Systems with cadmium-lined rods 69

4.5 Final remarks and conclusions 74

REFERENCES 77

LIST OF SYMBOLS 81

LIST OF ABBREVIATIONS 83

SUMMARY 84

SAMENVATTING 87

ACKNOWLEDGEMENTS 90

1. INTRODUCTION

In 1967 a Panel on Fuel Burn-up Predictions in Thermal Reactors formulated several requirements on burn-up physics, inter alia:

> The actual reactor flux distribution should be predicted well enough so that design tolerances are not set by (the error in) reactor physics models [1, p.233]; to operate at high power densities, it is essential to determine the hot-spot conditions accurately and the locations of the hot spots as a function of time [1, p.170].

Many calculations for heterogeneous thermal reactors make use of few-group two- or three-dimensional neutron diffusion theory. Energy- and space averaged cross-sections are obtained from more sophisticated lattice-cell calculations. The thermal neutrons are of particular importance in the calculation because the bulk of the reactions occurs in the thermal energy range. Since the spatial variation of the thermal spectrum over a cell is rather large, the averaged quantities for thermal neutrons must be calculated very carefully.

Much work has been done in the field of regular lattices. Computer codes like THERMOS [55] (which solves the integral transport equation) have been in common use for several years. As regards non-uniform lattices the situation is not so favourable. Unfortunately, all present-day power reactors have a non-uniform lattice structure. In boiling water reactors (BWR), for instance, water gaps exist between matrices of fuel pins (see Fig. 1.1). These gaps cause a local flux peaking, which affects the maximum permissible heat output of the reactor. The introduction of a control blade in a water gap alters the flux profile and hence the location of the hot spot. The control blade also increases the local ratio of epithermal-to-thermal neutron flux, which

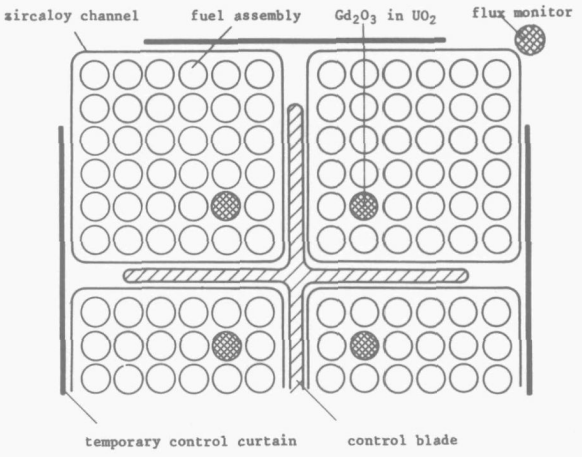

Fig. 1.1 BWR lattice configuration

causes increased conversion or plutonium production per unit of fuel burn-up. Furthermore,the absorptions in the control blade increase with decrease in water density; thus control absorbers have a negative effect on the temperature and void coefficients of reactivity.

Accurate description of the space- and energy dependent neutron flux in non-uniform lattices is thus important for economic as well as safety reasons. The above-mentioned Panel agreed upon a target accuracy of 5% in the prediction of local reaction rates at all sensitive locations. This target accuracy has since been scaled down to $\sim$ 2% as increase of reactor power of only a few per cent yields a substantial economic profit.

At the BNES Conference on the Physics Problems in Thermal Reactor Design (1967), Aline et al. [2] presented data on power distributions in BWR lattices. Two-dimensional diffusion theory calculations were performed, neglecting the space dependence of the spectrum caused by the water gaps. Differences of 10 to 16% with experimental data were found. When spectrum variations and transport theory corrections near the water gaps were taken into account the differences could be reduced to 5%.

This example is typical of the situation as it was some years ago, viz. reactor physics could predict the important physics parameters of non-uniform lattices by means of a rather simple model with an accuracy of about twice the desirable accuracy, whilst the predictions could be improved by corrections, mainly based on experience gained with operating reactors and subcritical experiments. Two-dimensional diffusion theory, using space-independent homogenised cross-sections from a uniform lattice calculation like THERMOS, was commonly used, as Honeck reported in a survey paper presented at a Symposium on Neutron Thermalization and Reactor Spectra in 1967 [3].

Meanwhile indications were obtained that an increase of accuracy should be sought in a more accurate account of the geometry rather than in the improvement of nuclear events and the neutron energy distribution [2]. In this respect the two-dimensional integral transport theory program CLEF [4,5] seemed a promising improvement. This program has, however, limited input capability as regards the geometry of the subject fuel cell assembly.

When formulating the scope of this thesis it was therefore decided that the work involved should lead to the development of a computer code which could handle *all* current fuel cells (BWR box cell, PWR cell etc.). Integral transport theory was chosen as the mathematical basis for the code because only with this theory did it seem possible to treat complex geometries "exactly". Moreover, the Reactor Physics Group in Delft had already considerable experience in developing integral transport codes (e.g. THERMOSQUARE [6] and PPIXY [7]).

Although one can gain much confidence in the reliability of a calculation model by comparison with other sophisticated models, the ultimate test of its results is provided by comparison with experimental results, as not only the model but also the nuclear constants (cross-sections) used in a calculation can cause inaccurate results. It was therefore felt that the code to be developed should be verified by means of some well-selected experiments. Here, we can distinguish two techniques involving (a) integral measurements (foil activation techniques) and (b) differential measurements (time-of-flight technique). Both techniques had been applied earlier in Delft by Caspers [8], but it was

felt that several adjustments had to be made to meet the required accuracy of the measurements in the more complicated systems to be investigated.

Integral measurements were and are still being performed by several investigators [39, 46, 47, 49, 50, 51, 52]; the accuracy of these measurements is nowadays within 2%. The energy solution is small as space-dependent reaction rates integrated over the energy are measured. Time-of-flight measurements of the space *and* energy dependent neutron flux constitute the ideal way of verifying the calculation models but are difficult to perform and to interpret, mainly because of the spectrum perturbation caused by the neutron beam extraction hole (probe tube). There is therefore a tendency among several investigators to restrict the experimental verification to integral measurements only [9,10].

By a suitable choice of the dimensions of the probe tube (i.e. rectangular cross-section with one side much longer than the other), its perturbation can be described exactly by a two-dimensional code [11]. Time-of-flight measurements using such a probe tube have therefore been included, thus obtaining neutron beams from systems which, on the one hand, could be treated numerically with adequate accuracy and, on the other hand, provided a severe check on the predicted neutron spectra.

Since the experiments primarily relate to the verification of a calculation model, the materials used in the measurements and calculations need not be realistic reactor materials. In order to avoid high activation levels, iron has been used to simulate uranium since the two materials have similar absorption- and scattering cross-sections.

The two-dimensional computer program developed in the course of this work has been baptized THERMOGENE. In an initial version isotropic scattering was assumed. Although the first measurements showed fairly good agreement with theory, some differences were observed, mainly in situations in which large flux gradients occur, and it was supposed that the assumption of isotropic scattering did not establish an adequate physical model. One-dimensional calculations with and without the inclusion of anisotropic scattering also indicated that differences might occur which could not be neglected. Therefore, THERMOGENE was extended so that anisotropic scattering could be taken into account.

The agreement between theory and experiment was indeed improved by this refinement.

In Chapter 2 the theoretical background of the THERMOGENE program and the principles of the treatment of arbitrary two-dimensional geometries will be described. Some calculated results are given and compared with other computer programs. A possibility of determining the accuracy of the numerical results is discussed.

Chapter 3 describes the experimental methods and the rearrangements in the instrumental set-up that had to be made to meet the required accuracy of the measurements.

In Chapter 4 a comparison is made between calculations and measurements which provides the ultimate check of the computational models.

2. CALCULATION METHODS

2.1 INTRODUCTION

This chapter describes the theoretical background of the developed THERMOGENE programs. They are based on the integral form of the transport (Bolzmann) equation, for the following reasons:

- In the systems under consideration with discontinuities and large flux gradients, transport theory must be used; diffusion theory is clearly not accurate enough;
- Transport methods based on the integro-differential form of the transport equation, such as the S_N method [56] suffer from the fact that the geometry of the systems must be divided by uniformly spaced mesh lines for the numerical calculation. In BWR lattices some homogenization must be applied to the geometry before an S_N calculation can begin.
- The angular dependence of the flux is treated exactly when integral transport theory is used, so that no approximating assumptions in regard to this dependence need be made, as for instance must be done in a P_N or S_N treatment of the transport equation. In the integral transport equation assumptions need only be made concerning the scattering of neutrons, viz., isotropic, linear anisotropic, etc. Unfortunately, the number of equations that must be solved in a numerical calculation increases drastically when higher order anisotropic scattering effects are taken into account. Most computer codes assume isotropic scattering (with some transport correction), which is adequate for a large variety of geometries, as has been shown by Honeck [12,36] and Takahashi [37].

In Section 2.2 the integral transport equation for linear anisotropic scattering for two-dimensional systems is formulated in a general way, i.e. without paying attention to the manner in which space is discretized. Some comments are made on the treatment of several boundary types in lattice cells.

The numerical solution of the integral transport equation requires the geometry of the system under consideration to be divided into small regions in which the flux is assumed to be constant. In complex geometries these regions may have different shapes. However, they must be identified in some way, so that the regions in which neutrons collide can be registered by the computer program. Sect. 2.3 more specifically deals with the key problem in the development of THERMOGENE, viz. the discretization of space in arbitary two-dimensional systems. In view of the complexity of the program only the principles of this treatment are mentioned. Full details can be found in the program report of THERMOGENE [13]. Also numerical methods used in the program are dealt with in more detail in the reports [13] and [14]. The program has been written in FORTRAN IV for the IBM 360/65 computer.

The introduction of flat-flux regions influences the accuracy of the results. A large number of small regions needs a great deal of computing time; the memory capacity of the computer may also be a limiting factor. In order to tackle this problem a procedure was developed to determine the numerical accuracy of the calculations within the computer. This procedure is described in Section 2.4.

In Section 2.5 some calculated results are presented and compared with other calculation models.

2.2 THE TWO-DIMENSIONAL INTEGRAL TRANSPORT EQUATION FOR LINEAR ANISOTROPIC SCATTERING; THE THERMOGENE PROGRAM

The space-, energy- and angle-dependent thermal neutron flux $\Phi(\underline{r},E,\underline{\Omega})$ is made up of contributions by sources at $\underline{r}'$ on a line through $\underline{r}$ in the negative direction of $\underline{\Omega}$ (see Fig. 2.1):

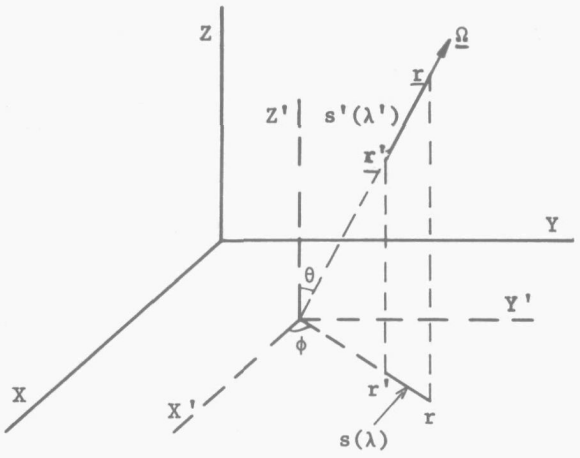

Fig. 2.1 Co-ordinate system for the angular neutron flux $\Phi(\underline{r},E,\underline{\Omega})$. λ' and λ are optical distances.

$$\Phi(\underline{r},E,\underline{\Omega}) = \int_0^{\infty} e^{-\lambda'(s',E)} ds' \left[S(\underline{r}',E,\underline{\Omega}) + \right.$$

$$\left. + \int_{4\pi} d\underline{\Omega}' \int_0^{E_c} dE' \Sigma^s(\underline{r}',E' \rightarrow E, \underline{\Omega}' \rightarrow \underline{\Omega}) \Phi(\underline{r}',E',\underline{\Omega}') \right] . \qquad (2.1)$$

$e^{-\lambda'}$ is the probability for neutrons born at $\underline{r}'$ to reach $\underline{r}$ without collisions; $\lambda' = \int_0^{s'} \Sigma^t(\underline{r}',E) d\underline{r}'$, i.e. the number of mean free paths between $\underline{r}$ and $\underline{r}'$ (Σ^t = total cross-section). $\Sigma^s(\underline{r}',E' \rightarrow E, \underline{\Omega}' \rightarrow \underline{\Omega})$ is the macroscopic cross-section at $\underline{r}'$ for neutrons with energy E' moving in direction $\underline{\Omega}'$, which are scattered in direction $\underline{\Omega}$ with energy E. E_c is the thermal cut-off energy above which upscattering is neglected. $S(\underline{r}',E,\underline{\Omega})$ is the external source which includes neutrons that are slowed down from above E_c into the thermal energy region.

Eq. (2.1) can be solved in principle for a given source distribution. It contains the complex differential scattering cross-section which makes a direct analytical solution impossible for realistic cases. For that reason Σ^s (and the flux and source) is expanded in a series of Legendre polynomials of the angular variable.

By a proper integration over the angular variable, expressions can be derived for the coefficients of the polynomials in the flux expansion.

The following simplifications will now be made:

- Only the first two terms in the expansion of the scattering cross-section (and the source term) will be retained, i.e. linear anisotropic scattering is assumed.
- The transport equation will be applied to two-dimensional systems, invariant in the z direction, which means for instance that $\lambda' = \lambda/\sin\theta$ (Fig. 2.1).

With these assumptions the following set of coupled equations is obtained (see also Fig. 2.1) *):

$$\Phi(r,E) = 2\int ds \int d\phi \Big[H_o(r',E)Ki_1(\lambda) + H_1(r',E)\cos\phi\ Ki_2(\lambda) + H_2(r',E)\sin\phi\ Ki_2(\lambda) \Big], \tag{2.2a}$$

$$J_x(r,E) = 2\int ds \int d\phi \Big[H_o(r',E)\cos\phi\ Ki_2(\lambda) + H_1(r',E)\cos^2\phi\ Ki_3(\lambda) + H_2(r',E)\cos\phi\ \sin\phi\ Ki_3(\lambda) \Big], \tag{2.2b}$$

$$J_y(r,E) = 2\int ds \int d\phi \Big[H_o(r',E)\sin\phi\ Ki_2(\lambda) + H_1(r',E)\sin\phi\ \cos\phi\ Ki_3(\lambda) + H_2(r',E)\sin^2\phi\ Ki_3(\lambda) \Big], \tag{2.2c}$$

where

$$\Phi(r,E) = \text{total flux} = \int d\underline{\Omega}\ \Phi(r,E,\underline{\Omega}), \tag{2.3a}$$

$$J_x(r,E) = \text{current in x direction} = \int d\underline{\Omega}\ \Phi(r,E,\underline{\Omega})\sin\theta\ \cos\phi, \tag{2.3b}$$

$$J_y(r,E) = \text{" " y direction} = \int d\underline{\Omega}\ \Phi(r,E,\underline{\Omega})\sin\theta\ \sin\phi, \tag{2.3c}$$

$$H_o(r,E) = \frac{1}{4\pi}\left[\int dE'\ \Sigma_o(r',E'\to E)\Phi(r',E') + S_o(r',E) \right], \tag{2.4a}$$

$$H_1(r,E) = \frac{3}{4\pi}\left[\int dE'\ \Sigma_1(r',E'\to E)J_x(r',E') + S_x(r',E) \right], \tag{2.4b}$$

$$H_2(r,E) = \frac{3}{4\pi}\left[\int dE'\ \Sigma_1(r',E'\to E)J_y(r',E') + S_y(r',E) \right]. \tag{2.4c}$$

---

* Eqs. (2.2) to (2.6) are given mainly to show how the formula for the transport kernel, Eq. (2.7), is derived.

Σ_o and Σ_1 are the 0^{th} and 1^{st} moment of the scattering cross-section. S_o, S_x and S_y are the first moments of the source $S(r,E,\underline{\Omega})$, defined analogously to, respectively, Φ, J_x and J_y in Eqs. (2.3).
$Ki_n(\lambda)$ is the well-known Bickley function:

$$Ki_n(\lambda) = \int_0^{\pi/2} d\theta \, \sin^{n-1}\theta \, \exp(-\lambda/\sin\theta) . \qquad (2.5)$$

It is worth mentioning here that one is interested primarily in the total flux $\Phi(r,E)$, which determines the various reaction rates. To find this quantity one has to calculate the currents J_x and J_y too. If isotropic scattering (and an isotropic source) is assumed, Eqs. (2.2) are reduced to the commonly used integral transport equation in which only the total flux is present. In Eqs. (2.2) no current in the z-direction appears; this current should indeed vanish in a two-dimensional system.

The set of equations (2.2) can be solved numerically in the usual way by introducing spatial regions $\Delta\underline{r}$ of constant flux and sources (indices n,i; total number: No) and energy intervals ΔE of which the midpoints are representative (indices j,k; total number: Ko). The integration over s can be effected immediately.
Integration over $\Delta\underline{r}_n$ finally results in (see Fig. 2.2):

$$\Phi_{\ell nk} = \sum_{i=1}^{No} \sum_{m=o}^{2} T_{m\ell nik} \, H_{mik} \quad , \quad \ell = 0,1,2 \quad n = 1 \text{ to } No \quad k = 1 \text{ to } Ko \qquad (2.6)$$

with

$$\Phi_{onk} = \frac{1}{4\pi} \Phi(r_n,E_k)$$

$$\Phi_{1nk} = \frac{1}{4\pi} J_x(r_n,E_k)$$

$$\Phi_{2nk} = \frac{1}{4\pi} J_y(r_n,E_k)$$

$$H_{mik} = H_m(r_i,E_k)$$

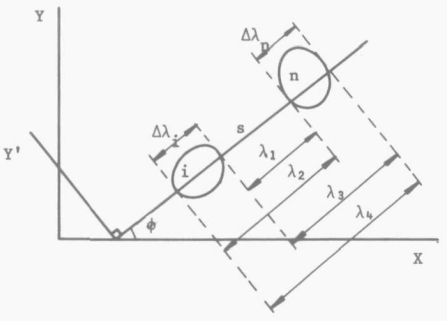

Fig. 2.2 Co-ordinate system for the transport kernel in a two-dimensional system.

and transport kernels $T_{m\ell nik}$ defined as

$$T_{m\ell nik} = \frac{1}{2\pi \Sigma^t_{nk} \Sigma^t_{ik} V_n} \int_0^{2\pi} d\phi \cos^i\phi \sin^j\phi \int dy' \, Ki^*_{3+i+j} , \qquad (2.7)$$

with

$$Ki^*_n = Ki_n(\lambda_1) - Ki_n(\lambda_2) - Ki_n(\lambda_3) + Ki_n(\lambda_4) ,$$

$$i = \delta(m-1) + \delta(\ell-1)$$
$$j = \delta(m-2) + \delta(\ell-2)$$

$$\delta(x) \begin{cases} = 1 \text{ for } x = 0 \\ = 0 \text{ for } x \neq 0 \end{cases}$$

V_n = area of region n.

The "self-collision" terms $T_{m\ell nnk}$ have a slightly different form, but consist also of a two-fold integral [14].

The transport kernels are evaluated numerically by placing over the geometry a set of parallel lines of constant spacing $\Delta y'$ at a set of angles between 0 and π which differ a constant value $\Delta\phi$. On these lines, which can be considered as neutron paths projected on to the x-y plane, λ-values are calculated for each pair of zones traversed by the line. With these λ-values Bickley function values are obtained by interpolation between two tabulated values.

For the solution of Eq. (2.6) the scattering kernel and the source term should also be known. The scattering kernel is obtained with the SCAM program [15]. In this work, light water and polyethene were used as moderators. For water the Koppel-Young scattering model was used [16], which is an improved version of the Nelkin model [17]. For polyethene the Goldman model was used [18]. Several investigators [8, 10, 19] have shown that these models provide an accurate description of the thermalization process. The source term, consisting of neutrons slowed down into the thermal energy range from epithermal energies, can be calculated provided the epithermal neutron spectrum is known. This spectrum is usually supposed to be proportional to 1/E. Slight deviations from this 1/E behaviour do not seriously affect the source term [10].

Once the scattering kernel, the source term and the transport kernel are known , Eq. (2.6) can be solved numerically, using the well-known Gauss-Seidel iteration technique with overrelaxation and normalization. Angular spectra $\Phi(r,E,\underline{\Omega})$ can be calculated afterwards, using Eq. (2.1).

Two programs have been written, viz. THERMOGENE I which only can handle isotropic scattering, and THERMOGENE II, in which linear anisotropic scattering is included.

A few words should be said here about the treatment of the boundary of a lattice-cell. Lattice-cell calculations normally deal with systems consisting of a large number of identical cells. The boundary of a cell will then consist of planes of symmetry. Only one cell requires to be considered, provided the neutrons are "reflected" at the cell boundary. Expressions for the transport kernels for "reflected" neutrons have been derived in the program report [14]. When a boundary of the cell consists of a control blade the neutrons that reach this boundary are absorbed and will not return into the cell. Both types of boundary, i.e. perfectly reflecting and black boundary, are incorporated in THERMOGENE I as well as in THERMOGENE II. A third boundary type, the isotropic flux return, is incorporated in THERMOGENE I. It is commonly used in THERMOS calculations where the square or hexagonal cell boundary is replaced by a circular one; it gives a more accurate prediction of the flux profile than a perfectly reflecting boundary would do because of the approximation in the geometry description [12,20]. In relation to the perfectly reflecting boundary it gives a large reduction in the calculation time of the transport kernels, since the isotropic reflection can be incorporated mathematically in the calculation so that the neutrons need not be followed after reflection. The isotropic flux return was first suggested by Honeck [21]; its mathematical treatment was improved by Carlvik [22]. It can be used to advantage in THERMOGENE provided the flux near the cell boundary is fairly flat.

It will be clear that in Eq. (2.6) the aspects of neutron transport and hence of lattice geometry are found in the transport kernel. In the next section the aspects of lattice geometry in the calculation of this kernel will be studied.

2.3 TREATMENT OF ARBITRARY TWO-DIMENSIONAL GEOMETRIES IN THERMOGENE

The numerical solution of the integral transport equation for an arbitrary two-dimensional system (e.g. a BWR box cell surrounded by control blades and/or water gaps) requires the geometry of the system to be divided into small regions.Fig. 2.3 shows an example of such a division of one half of a box cell. In one-dimensional systems it is no problem to define such regions; in slab systems they are numbered, e.g., from left to right and are bounded by parallel planes. In arbitrary two-dimensional systems such regularity does not exist: the regions may have all kinds of shapes and must often be numbered in a rather disordered way.

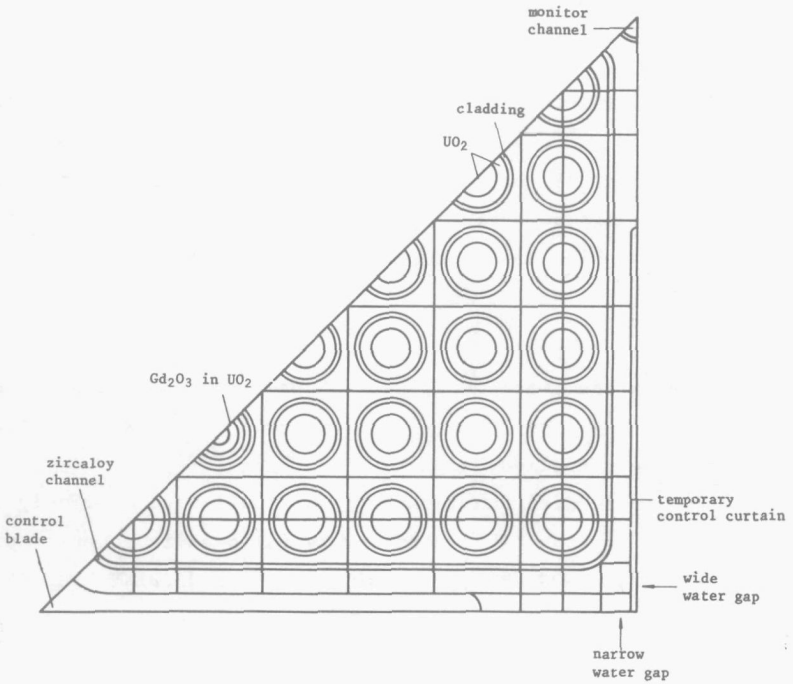

Fig. 2.3 Example of the division of space of a BWR lattice, applied in the numerical solution of the transport equation.

In Sect. 2.2 it was shown that the calculation of the transport kernels requires that lines (representing projected neutron trajectories) are drawn over the geometry for particular ϕ and y' values, and optical lengths between the regions traversed by the lines have to be calculated, so that the kernels can be found by a proper combination of Ki_n values. In view of this procedure to be followed, it will be clear that the following problems arise for arbitrary two-dimensional geometries:

a. The complete picture of the geometry should be known to the computer program. Moreover, all regions should be known, i.e. the regions should be numbered in some way and the program must know their shape and where they are located. In other words, the boundaries of each region must be known.
   The definition of the geometry of all the regions by the user requires an inconveniently large amount of input data. In practice, the number of regions will generally be 200 or more.
b. The intersecting sequence of the regions by a projected neutron trajectory must be found in some way, i.e. not only the optical distances cut off by the region boundaries should be known, but also the region numbers belonging to these optical distances. In slab systems this problem does not exist at all, since neutrons travelling from left to right and having left region n will simply arrive in region n + 1.

In some existing two-dimensional integral transport codes attempts have been made to by-pass or to alleviate these problems. The following solutions have been applied:

- Only a very simple division into regions is allowed, e.g. only square or rectangular regions. This strategy is followed in computer programs like BOCOP [23], MINOS [24], THERMOSQUARE [6] and PPIXY [7]. It will be clear that in such programs some homogenization of the materials present in realistic systems is needed in most cases.
- Division into regions is allowed according to certain specified rules so that the regions can be defined by the program in a systematic way. For instance, in the CLUCOP code [25] the geometry is subdivided by concentric circles on which uniformly spaced mid points of other

circles may be situated. Only certain types of fuel elements can be treated with such a program.

In the present work the division into regions is allowed without any essential restriction. The geometry may be divided by straight lines and/or circles in an arbitrary manner. Only the parameters of these lines and circles need be supplied by the user of THERMOGENE. The program itself provides for a systematic numbering and identification of the regions. The materials present in the regions (H_2O, UO_2, etc.) should of course be given by the user.

Below some details of the geometry treatment in THERMOGENE will be mentioned.

Systematic construction of the geometry

A program called GEOTRY, which is incorporated in THERMOGENE, constructs a two-dimensional geometry from a given set of straight lines and circles that constitute the region boundaries. These boundaries are numbered by the program in some systematic way. The regions are identified by the numbers of their boundaries and the way in which they are bounded, i.e. either inside or outside a circle, and at one of the two sides of a straight line. As a rule, a point is situated in either the "positive" or the "negative" area of a line depending upon whether a positive or a negative result is obtained when the co-ordinates of this point are substituted in the equation of the line, the equation of a straight line and a circle being, respectively, $-x \sin\phi + y \cos\phi + c = 0 (0 \leq \phi < 180^{\circ})$, and $(x - x_o)^2 + (y - y_o)^2 - r^2 = 0$. In Fig. 2.4, e.g., region No. 4 is completely described by the fact that it is in the negative area of line No. 2, in the positive area of line No. 5 and the negative area of circle No. 8.

The regions are numbered and identified systematically in the following way:

(a) All intersections of the region boundaries are determined and numbered in rising values of their y co-ordinates and for the same y co-ordinate in rising values of their x co-ordinates. This numbering is shown in Fig. 2.4.

(b) The intersections on a region boundary are numbered separately for each boundary. For straight lines this numbering is in the same order as is the case under (a), whilst for circles the intersections are numbered according to their position on the circle, clockwise.

(c) Each intersection (1,2,....) is used as a possible starting point for the definition of one or more regions. The boundaries of a region are tracked anticlockwise, running from vertex to vertex. At each vertex a new direction, more precisely the left-hand direction, is chosen until a closed loop has been made.

(d) When a boundary is followed and the next vertex has a higher (lower) index than the

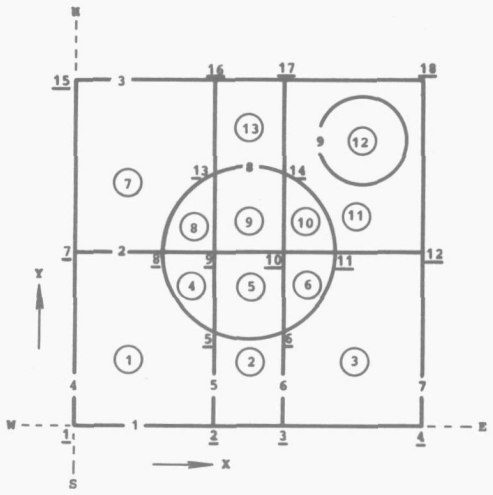

Fig. 2.4 Example of the identification of the regions in a two-dimensional system. The numbers of the region boundaries have been inserted. The underscored and encircled numbers indicate the numbering of the intersections and the regions, respectively.

preceding one according the numbering of (b), the region is situated in the positive (negative) area of this boundary.

(e) An intersection will only be used as a starting point when one or more vertices with a higher index (according to the numbering of (a) and of Fig. 2.4) can be reached via more than one direction. The leftmost of these directions (relative to the positive x axis) is not used as a starting direction, from the remaining directions the leftmost one is used first, the rightmost one last (from left to right means, in Fig. 2.4, S→W→N→E→S). In Fig. 2.4 this rule is applied in the definition of regions 4 and 5, both obtained from intersection No. 5 as starting point.

(f) The formula for the transport kernels (Eq.(2.7)) contains the areas of the regions. These areas are obtained simultaneously with the definition of a region when a boundary is followed from vertex to vertex by integrating analytically the equation of the line.

The formulations outlined above can be used for many geometries. Nevertheless, the system is less general than it should be. For a number of cases which would cause trouble, provisions are made in the program. Some of them will be mentioned here:

(a) Circles which are not intersected by any other region boundary would not be encountered when using the above-mentioned procedure. They are examined in a separate subroutine. In Fig. 2.4 this subroutine would have defined region No. 12.

(b) In some cases a region is not identified solely by its boundaries. In Fig. 2.4,

for instance, points in region No. 13 also fulfil the requirements of region No. 2, viz. above line No. 1, between lines 5 and 6 and outside circle No. 8. In this case an extra boundary is specified for region No. 2, viz. the straight line through intersections 5 and 6.

It may be said that, with these provisions, the GEOTRY program can handle all practicle geometries and they may be divided into regions without any essential restriction. The calculation time of the GEOTRY program for complex geometries is in the range of 30 seconds.

Geometry aspects in the calculation of transport kernels

When a line is set across the geometry for the calculation of the transport kernels, the distances cut off by the region boundaries can be calculated quite simply. A more difficult problem is the determination of the region numbers belonging to each line segment. This is done in principle by taking the mid point of a segment and testing whether this point fulfils the specifications of region 1, 2, 3 etc. Since a geometry will normally consist of more than a hundred regions, this searching routine would take a great deal of computing time. Several possibilities exist to speed up this searching routine:

(a) The first region which is traversed by the line will always be a region at the boundary of the geometry. When the boundary regions are stored separately, the program need only check against these regions to find the first intersected region.

(b) The next region traversed by the line will be one of the neighbours of the first one. When the neighbours of each region are stored, the program need only check against these neighbours to find the next intersected region (regions are neighbours when they have one or more vertices in common).

With these refinements the searching routine takes only a minor part of the total calculation time of the transport kernels.

2.4 EFFECT OF DISCRETIZATION ON THE ACCURACY OF CALCULATED RESULTS

The introduction of discrete regions and energy intervals affects the calculated space-dependent neutron spectrum. The limiting case of infinitely small regions and energy intervals will produce the correct spectra, but computer memory and calculation time will limit the maximum permissible number of steps.

As regards the number of energy intervals, a detailed investigation has been carried out by Caspers [8] from which some results can be taken which are of interest for the present work:

- a division of the thermal energy range into 10 intervals will produce spectra in water systems with an accuracy about 2 to 3%. A thermal cut-off energy of 0.63 eV is sufficiently high although some up-scattering occurs above this energy which results in too low values of the spectrum near 0.6 eV.
- in polyethene systems the number of energy groups must be enlarged in order to arrive at the same accuracy. Also the cut-off energy should be greater than 0.63 eV, at least 1 eV.

Throughout this work 10 energy groups and a cut-off energy of 0.63 eV were used if water was the only moderator. If polyethene was present 21 groups were used with a cut-off energy of 1.24 eV.

It is almost impossible to observe a regularity in the deviations caused by the introduction of more or less energy groups. This must be due to the straggling curve of the differential cross-section, caused by the vibration energy levels of the H_2O or CH_2 molecule.

A study of the influence of the spatial discretization shows a systematic deviation, viz. that larger flat-flux regions cause a smoothening of the flux profile. When neutrons are scattered inside a region they are spread out uniformly over the region before their contribution to the flux in other regions is calculated; in this way neutrons are transported from points with a higher flux to points with a lower flux. This transport, introduced by the mathematical treatment of the transport equation, causes too small flux variations in a system.

Another method for the solution of Eqs. (2.2) is based on a point-wise representation of space, i.e., the mid points of the spatial regions are considered to be representative of the whole region. In this treatment neutrons that are scattered are concentrated at the mid point of a region before they start again. Since the coupling between the regions is thus reduced the flux variations in a system will be too large.

The effect of these two extreme representations of the transport equation has been examined for a one-dimensional cylindrical system. The flat-flux representation is applied in the FLURIG program developed by Carlvik [4]. For the point-flux representation a program has been written which is based upon the DIT-method developed by Carlvik [22]; it is called DIT-DELFT [26]. Both programs apply a one-group repre-

sentation of the thermal neutrons.

Fig. 2.5 shows the geometry of the cylindrical cell. It consists of 1 cm thick shells of absorber and moderator (iron and light water) with absorption cross-sections 0.487 cm^{-1} and 0.015 cm^{-1} and scattering cross-sections 0.913 cm^{-1} and 2.0 cm^{-1}, respectively. Single-cell calculations were performed, i.e. a black outer boundary was assumed.

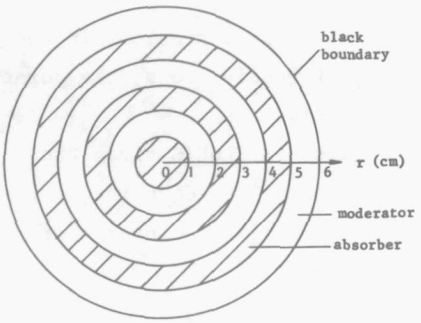

Fig. 2.5 Cylindrical cell system used for the study of the effect of various transport models.

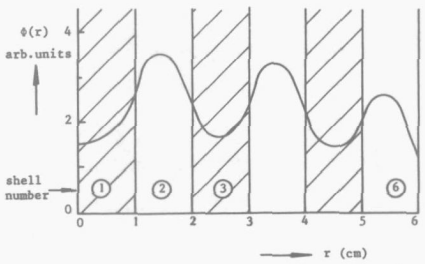

Fig. 2.6 Flux profile in the cylindrical cell system.

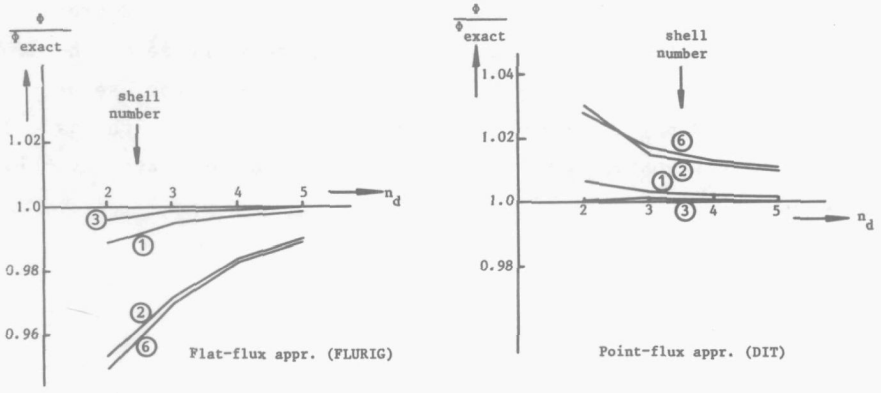

Fig. 2.7 Flux deviation from "exact" value, as a function of n_d, the number of subdivisions per shell. Φ_{exact} is shown in Fig. 2.6. Two transport models, the flat-flux approximation and the point-flux approximation, have been used.

The number of regions (space points) per shell was varied from 2 to 5. Fig. 2.6 shows the flux profile over the cell obtained with the most accurate calculation.

In Fig. 2.7 the variation is shown of the mean flux in the shells as a function of the number of regions (space points) per shell. The following observations can be made:

(a) The FLURIG and the DIT calculations tend to the same results when the number of subdivisions is increased.

(b) The flat-flux approximation shows too small flux variations in the heterogeneous system for a finite number of subdivisions; the point-flux approximation shows too large flux variations.

(c) The total flux in the cell is underpredicted by FLURIG since the neutron leakage from the cell is overpredicted (the coupling between the shells and the black boundary is too strong). The inverse argumentation applies to the DIT calculation.

The following conclusion may be drawn: when the number of regions must be kept small because of computer memory capacity limitations, two calculations based upon both approximations give extreme values of the flux profile in the system and one can immediately make an estimate of the deviation from the true flux profile (for an infinite number of subdivisions).

The point-flux approximation can be applied quite simply in the THERMOGENE program. The mid points of $\Delta\lambda_i$ and $\Delta\lambda_n$ in Fig. 2.2 are assumed to be representative of regions i and n. The formulae of the transport kernels have to be modified, which results in the use of Bickley functions Ki_{n-2} instead of Ki_n (compare Eq. (2.7) with Eqs. (2.2)). Results of both transport models obtained with THERMOGENE are given in Sect. 2.5.

2.5 CALCULATED RESULTS OBTAINED WITH THERMOGENE

In analyzing numerical calculations one can distinguish between several aspects which may cause inaccurate results:

(a) The used basic data, i.e. the cross-sections. In the thermal energy region cross-sections are well known. Perhaps one should make an

exception for some fissile materials like ^{239}Pu. The use of inaccurate cross-sections can be detected only by comparison with experiments.

(b) The scattering models for the moderating materials. As stated in Sect. 2.2, the models applied in this work have been shown to give reliable results for well-thermalized spectra. The ultimate test of their reliability should also be provided by experimental verification.

(c) The approximation to the transport equation, applied in numerical calculations. An estimate of the errors introduced by this approximation can be obtained from a comparison with other approximations such as S_N calculations. Such a comparison is made below. The effect of the approximation to the scattering kernel, viz. the number of Legendre moments incorporated in the calculation, can be evaluated by comparison of calculations with one or more moments included. The evaluation of the effect of a finite number of energy and space steps has been described in Sect. 2.4, where it was shown that the effect of space discretization can be evaluated theoretically.

(d) The description of the geometry of the system under consideration. In THERMOGENE no approximations to this description are needed. Nevertheless , a comparison is made below with the CLUCOP program [23] in which also no homogenization is required. From this comparison one can gain an impression of the influence of the last source of inaccuracies:

(e) The numerical calculation of the transport kernels. These kernels are obtained by applying the trapezoidal rule to the double integral in Eq.(2.7) (Sect. 2.2). The accuracy of this calculation can be estimated by varying the number of lines placed across the geometry.

Fig. 2.9 shows some results of calculations with THERMOGENE for a system consisting of a square box of H_2O in vacuum in which 9 iron rods are submerged (see Fig. 2.8). The calculations are compared with results obtained with the two-dimensional diffusion theory program EXTERMINATOR-2 [27] and with S_N calculations performed with the SFINX program [28]

recently developed by Stamm'ler*). In the three types of calculation the system was divided into square regions of 4x4 mm^2. The same scattering kernel was applied in all calculations; isotropic scattering was assumed, anisotropic scattering was accounted for by the commonly used diagonal transport correction [10,12], and ten energy groups were used. The flat-flux approximation as well as the point-flux approximation were applied in the THERMOGENE calculations.

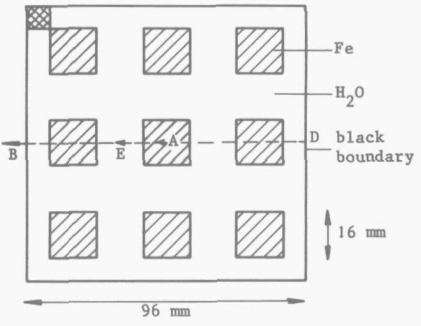

Fig. 2.8 Square box cell in vacuum used for the calculation of the neutron flux with various transport models. Calculated results are shown in Figs. 2.9, 2.10 and 2.11.

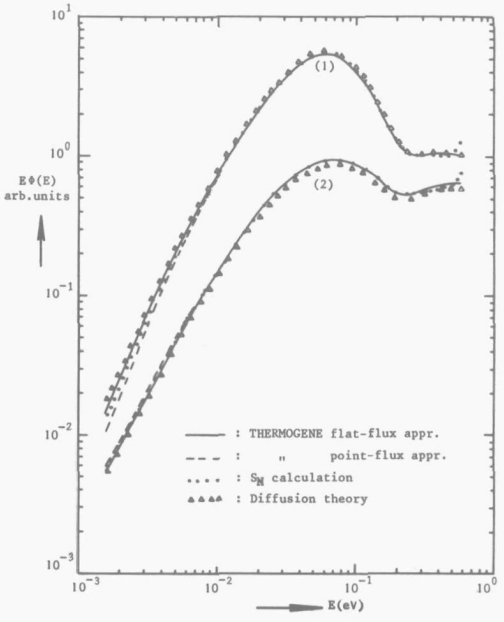

Fig. 2.9 Calculated scalar spectra $\Phi(E) = \int \Phi(E,\underline{\Omega})\, d\underline{\Omega}$ in the system of Fig. 2.8.
(1): space averaged spectrum in the central Fe rod.
(2): space averaged spectrum in the shaded H_2O region near the corner of the system.
The spectra have been normalized with respect to the source.

*Thanks are due to Stamm'ler, who kindly supplied the results of his SFINX program.

From the results shown in Fig. 2.9 the following conclusions can be drawn:

(a) Integral transport theory and S_N theory are in close agreement in predicting the space- and energy distribution of the thermal neutron flux. Although diffusion theory fairly well predicts the energy dependence of the flux, it fails to predict the space-dependence.

(b) THERMOGENE calculations are sensitive to the finite division of space. Below 0.1 eV the flux variations in the heterogeneous system are so large that the assumption of a flat flux in the 4x4 mm^2 regions leads to noticeable errors.

(c) Results obtained with SFINX generally lie between THERMOGENE results obtained with the two transport models. The differences between SFINX- and THERMOGENE results for high energies(>0.2 eV) are due to a different (and from a physical point of view rather dubious) treatment in SFINX of the negative diagonal elements of the scattering matrix (negative elements occur above 0.2 eV and are due to the diagonal transport correction). In EXTERMINATOR-2, which treats the diagonal elements correctly, this deviation above 0.2 eV is not observed.

The effect of spatial discretization in THERMOGENE can be studied in somewhat greater detail with the results shown in Figs. 2.10 and 2.11.

In Fig. 2.10 the scalar energy integrated flux along the line BA of Fig. 2.8 is shown. The THERMOGENE calculations have been repeated with a spatial discretization of $2\frac{2}{3}$ x $2\frac{2}{3}$ mm^2 regions. The conclusions drawn in Sect. 2.4 from the one-dimensional, one-group calculations also apply to the results shown in Fig. 2.9, e.g., the point-flux approximation predicts too large flux variations and too small neutron leakage from the system (too large total flux in the system). The difference between the results of both transport models amounts to 7% when regions of 4x4 mm^2 are used. Thus predicted integral quantities such as reaction rates are rather sensitive to the spatial discretization. When integral measurements, i.e. activation measurements, are compared with calculations, the effect of the spatial discretization should be evaluated accurately.

Fig. 2.11 shows angular spectra along the direction $\overrightarrow{DB}$ (ref. Fig. 2.8) at the positions (A), (E) and (B), calculated with a spatial mesh of 4 mm. Again, the point-flux approximation (PFA) predicts a too large flux

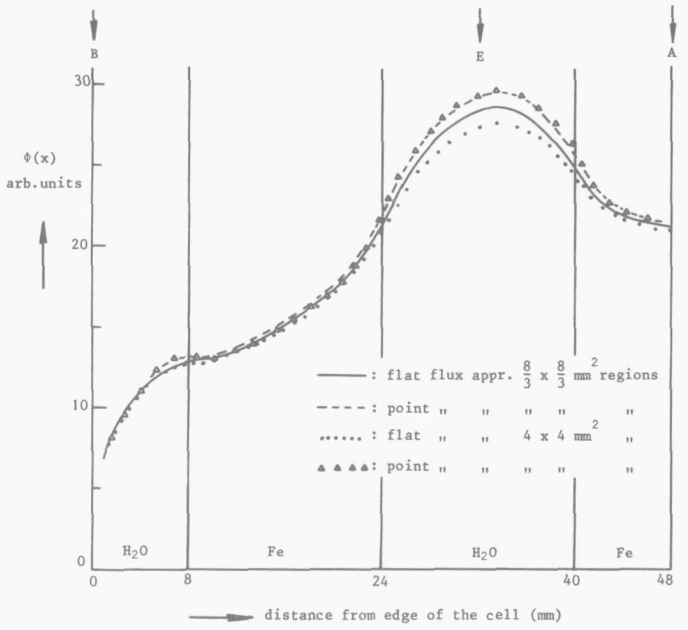

Fig. 2.10 Calculated scalar energy-integrated flux along the line BA of the system shown in Fig. 2.8.

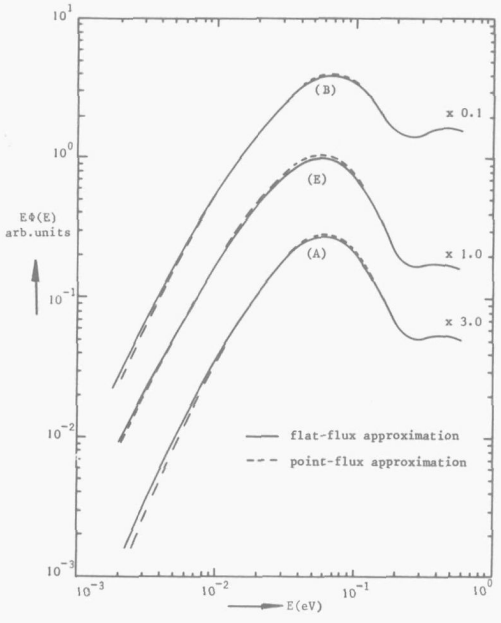

Fig. 2.11 Angular spectra along $\overrightarrow{DB}$ at positions (A), (E) and (B) (ref. Fig. 2.8).

variation over the system. In the energy region around 0.05 eV PFA predicts too high flux values which is consistent with the results shown in Fig. 2.10, as most neutrons have energies around 0.05 eV. The formalism for the numerical calculation of angular fluxes applied in PFA *) results in too low angular fluxes, as compared with scalar fluxes, especially when large neutron cross-sections are considered. For that reason PFA predicts too low angular fluxes below 0.01 eV, even at position (E) (the total cross-section of water becomes greater than 6 cm^{-1} below 0.005 eV, at 0.05 eV its value is about 2 cm^{-1}).

Except for energies below 0.005 eV the difference between the two transport models is less than 5%, even at position (E). The angular flux is made up of contributions of source neutrons on the line ED, so that the local difference of the scalar fluxes at position (E) is reduced in the angular fluxes. Angular spectra are thus less sensitive to the spatial discretization than scalar spectra; this fact can be used to advantage when calculations are compared with angular spectrum measurements.

The influence of anisotropic scattering effects can be examined with the results obtained from calculations with THERMOGENE I and THERMOGENE II for the system of Fig. 2.12, consisting of a square box cell in vacuum. Square regions of 4 x 4 mm^2 were used. In the isotropic scattering approximation the diagonal transport correction was applied. In both calculations the same isotropic source term was used. Fig. 2.13 shows the energy-integrated flux profile along the diagonal AC (see Fig. 2.12). In Fig. 2.14 the scalar flux spectrum $\Phi(E) = \int \Phi(E,\underline{\Omega})\, d\underline{\Omega}$ is shown for the shaded regions at position A and position C, together with the angular spectra emerging from the box cell at positions B and C.

From the results shown in Figs. 2.13 and 2.14 one can draw the following conclusions:

(a) Anisotropic scattering has a relatively larger effect on the detailed spectrum (maximum effect 3%) as compared with the energy integrated flux (maximum 1.5%). The effect is confined to energies above 0.1 eV; for lower energies the thermal motion of the moderating atoms becomes of the same magnitude as the neutron velocity.

(b) The effect is larger for the angular spectrum (maximum 7%) as compared with the scalar spectrum (maximum 3%): integration over the angle $\underline{\Omega}$ cancels to a certain extent the effect in the detailed angular

*) Here source neutrons are also concentrated at the mid point of a region.

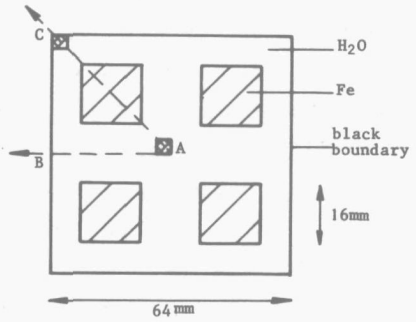

Fig. 2.12 Geometry used for the study of anisotropic scattering effects.

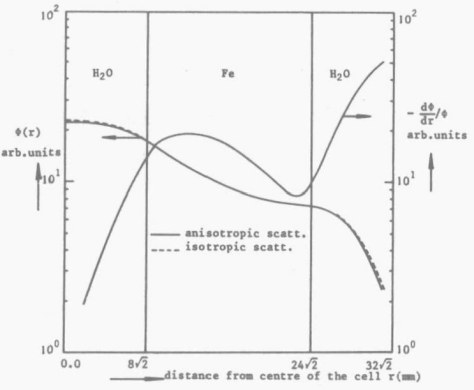

Fig. 2.13 Energy-integrated flux $\Phi(r)$ and $-\frac{d\Phi}{dr}/\Phi$ along diagonal AC (ref. Fig. 2.12).

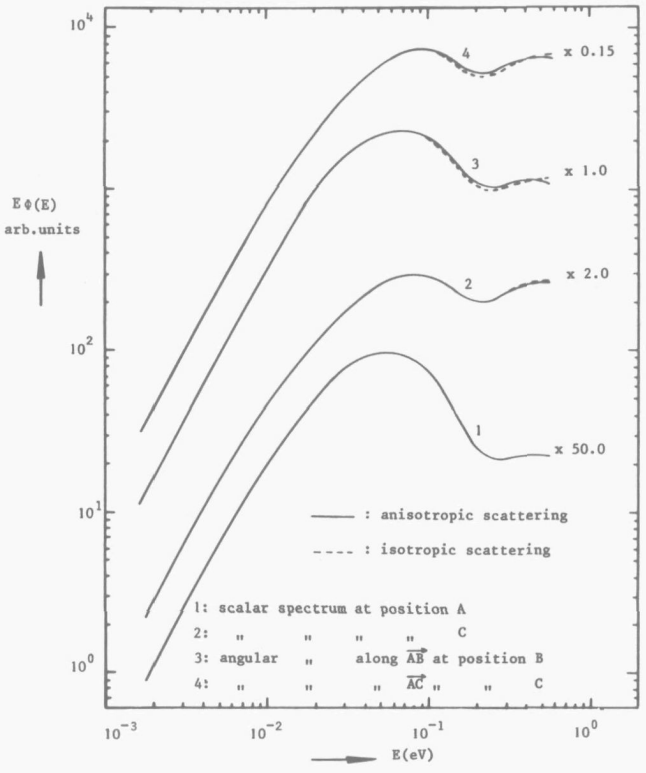

Fig. 2.14 Scalar and angular spectra in the system of Fig. 2.12.

spectrum. As reaction rates are determined by the scalar flux, the effect on the reaction rates is consequently relatively small. On the other hand, the number of neutrons absorbed in a control blade is determined by the angular flux. Therefore, for the prediction of the reactivity worth of control absorbers, anisotropic scattering generally cannot be neglected.

(c) Anisotropic scattering affects the neutron spectrum only when the flux is not constant in space. As a rule one can estimate the necessity of an anisotropic calculation to meet a given accuracy (of the angular, scalar or total flux) by comparison of the flux gradient and the total flux. From Fig. 2.13 it can be seen that the ratio of the flux gradient and the flux becomes very large near the black boundary of the cell.

The effect of inaccuracies in the numerically calculated transport kernels can be studied by comparison between one-group calculations with THERMOGENE for a Marviken boiler cell and results obtained with the one-group code CLUCOP. The cell consists of 31 fuel pins (diameter 1.26 cm) submerged in heavy water. The pins are divided into 4 groups of respectively 1, 5, 10 and 15 pins at increasing distance r_i from the centre of the cell (respectively at 0.0, 2.16, 4.31 and 6.41 cm from the centre). CLUCOP calculations have been described by Carlvik in ref. [23]. The same cross-sections as well as the same division into flat-flux regions were applied in THERMOGENE. Table 2.1 shows some results from calculations with different accuracies of the numerically obtained transport kernels. The distance between the lines placed across the geometry was kept constant at 0.2 cm, (in the CLUCOP calculation the distance was 0.225 cm), the number of angles between 0 and π was subsequently 6, 10 and 20. The integration over the angle was treated somewhat differently in CLUCOP; the accuracy of the CLUCOP values in Table 2.1 is in any case within 1%.

Comparison of the results recorded in Table 2.1 shows that both THERMOGENE and CLUCOP calculations tend to the same flux prediction when the accuracy of the transport kernels is increased. The convergence to the "exact" values is faster for pins at a larger distance from the centre owing to the fact that the area in which the flux $\bar{\Phi}_i$ is present increases for larger values of i, viz. 1 pin for $\bar{\Phi}_1$, 5

	$\bar{\Phi}_1$	$\bar{\Phi}_2$	$\bar{\Phi}_3$	$\bar{\Phi}_4$
THERMOGENE				
number of angles NP = 6	45.08	46.87	52.55	65.06
NP = 10	44.79	46.29	52.91	65.09
NP = 20	43.35	46.13	53.00	65.15
CLUCOP	43.59	46.345	53.02	65.095

Table 2.1 Effect of the accuracy of the numerical calculation of the transport kernels.
$\bar{\Phi}_i$ = average flux in pins at distance r_i from the centre of the cell (see text).

pins for $\bar{\Phi}_2$, etc. Consequently, the number of lines crossing the pins increases for larger values of r_i. The areas of the regions into which a system is divided should therefore be kept as equal as possible. Table 2.1 shows that a relatively coarse mesh of the network of lines already gives quite accurate results. From a set of parallel lines at a distance of 0.2 cm 6 or 7 lines cross one pin; the integration over the angle between 0 and π with only 10 steps already gives results good enough for many practical applications.

Summarizing, it may be stated that, bearing in mind the approximations to the transport equation, THERMOGENE gives a reliable prediction of the flux distribution. Angular spectra are rather sensitive to the effect of anisotropic scattering, whilst the effect of spatial discretization is smaller. As regards space-dependent reaction rates, the isotropic scattering approximation will generally be accurate enough, but the effect of spatial discretization is more pronounced and should be evaluated accurately.

However, before THERMOGENE can be used as a means for accurate prediction of space-dependent neutron spectra, the ultimate test of its reliability (regarding the approximations to the transport equation *and* the used cross-sections and scattering models) should be provided by comparison of its results with time-of-flight measurements of angular spectra and with measurements of reaction rates.

3. EXPERIMENTAL TECHNIQUES

3.1 GENERAL CONSIDERATIONS

When calculated neutron distributions are compared with measurements it is worth-while to distinguish between the space- and the energy distribution , for the reasons outlined in Sect. 2.5. Two basically different experimental methods lend themselves for a check on each aspect of the predicted distribution, viz.:

- measurements of detailed spectra with a time-of-flight spectrometer. A high energy resolution is combined with a moderate spatial resolution owing to the insertion of a neutron extraction hole which causes a spatial flattening of the flux.
- measurement of spectrum-sensitive quantities by means of activating foils or wires. A high spatial resolution can be obtained by selecting sufficiently small detectors; the energy resolution is essentially poor because of the fact that energy-integrated quantities are measured.

Although one can improve the spatial resolution of time-of-flight measurements by reducing the dimensions of the extraction hole, it is usual to examine spatial effects by means of integral measurements in order to avoid the many difficulties encountered in a time-of-flight measurement.

The energy resolution in integral measurements is set by the resolution with which various detector materials can distinguish neutron energies. Spectrum unfolding techniques, using three or more activation materials, should be applied very cautiously, as they can hardly bring out any resonance structure in the spectrum [48]. In this work the 1/v absorber ^{164}Dy was used as detector of the spatial neutron density

distribution, whilst a few measurements were performed, using the resonance detector ^{176}Lu which, in combination with ^{164}Dy, gives a reading of the "hardness" of the spectrum, i.e. the mean neutron energy*).

The following sections of this chapter are devoted to the two experimental techniques. Both techniques were applied in Delft before this investigation was started. This chapter will therefore be limited to a description of the changes that had to be introduced into the experimental set-up for accurate measurements in two-dimensional systems, and to the calibration of the spectrometer after the changes had been made. Further details of the experimental techniques can be found in ref. [8].

3.2 THE TIME-OF-FLIGHT SPECTROMETER

3.2.1 P r i n c i p l e

In the time-of-flight spectrometer a chopper transforms the continuous neutron beam from the experimental system into short pulses of neutrons (see Fig. 3.1). The experimental system is situated in the thermal column near the core of the HOR, the swimming pool reactor in Delft.

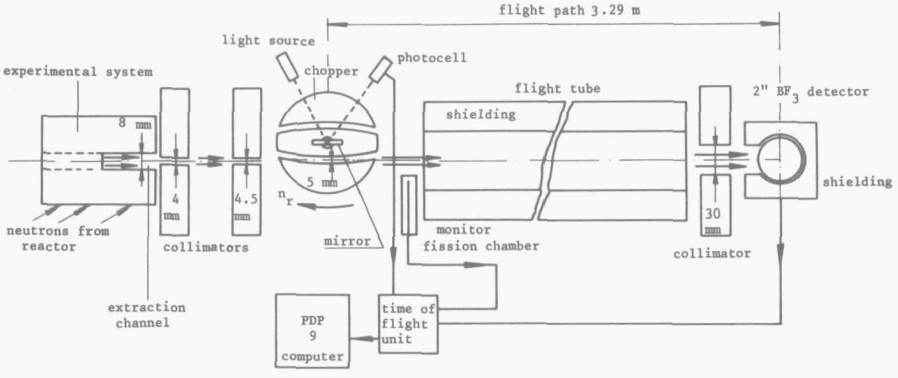

Fig. 3.1 The principle of the time-of-flight spectrometer.

* ^{176}Lu has a resonance peak in its activation cross-section at 0.142 eV.

The neutrons in the pulses travel a flight path l_f of 3.29 m before they are detected in the BF_3 counter. The velocity v of the neutrons follows directly from the measured flight time $t = l_f/v$. The chopper consists of K-monel and has a diameter of 20 cm. The slits in the chopper are designed in such a way that no neutrons are transmitted with flight times longer than the time elapsing between two pulses. The slits have a width of 5 mm, they are lined with cadmium to prevent the transmission of thermal neutrons through the chopper material, and they are curved (radius of curvature R = 1.46 m) in such a way that the maximum transmission occurs for thermal neutrons. The neutron beam is so collimated by a set of B_4C collimators that only neutrons from the bottom of the extraction hole can reach the detector. The time measurement is performed by a time-of-flight (TOF) unit containing an electronic clock which is started by means of the optical system indicated in Fig. 3.1. The TOF unit is connected with a PDP 9 computer. Neutron counts are added to specific core memory locations according to the neutron flight time. The time that has elapsed since the electronic clock was started is divided into a number of steps of a preset constant width (channel width).

The neutron flux $\Phi(t)$ can be calculated from the core memory contents w(t), using the relation

$$\Phi(t) = C \frac{w(t)-b(t)}{T(t)\ \varepsilon(t)\ N_m} g(t) \qquad (3.1)$$

where $b(t)$ = neutron background,

$T(t)$ = transmission of the rotor,

$\varepsilon(t)$ = efficiency of the detector,

N_m = correction factor to take into account the reactor flux and the measuring time,

$g(t)$ = correction factor to take into account the effect of the spectrometer resolution, the transmission through materials present in the neutron beam, and dead time count losses,

C = constant determined by the dimensions of the spectrometer.

3.2.2 Adaptation of the spectrometer

When this investigation was started the spectrometer was specially adapted for measurements in systems from which a rather rapidly diverging neutron beam could be extracted. The divergence of the neutron beam was such that 3 parallel rotor slits viewed the source area (only one is shown in Fig. 3.1) and 9 BF_3 counters were used for the detection of the neutrons.

For space dependent spectrum measurements a collimator had to be placed directly in front of the experimental system to confine the extracted neutron beam. Unfortunately the time-dependent background, caused mainly by fast neutrons scattered by the collimator, limited the accuracy of the experimental results.

Owing to the divergence of the neutron beam the source area viewed by the detectors rapidly increased with increasing distance between the collimator and the bottom of the extraction hole. For the present measurements it was necessary to obtain a source height of 5 mm at a distance of up to 20 cm from the collimator. In order to fulfil this requirement the pre- and after-collimators of the chopper were redimensioned in such a way that only one rotor slit viewed the source area, and only one BF_3 counter was installed in the detector bank.

In this configuration the background of fast neutrons was still much too high. This background could be reduced by introducing two extra B_4C collimators in the shielding between the experimental system and the chopper. These collimators acted as a shielding of the fast neutrons from the collimator directly in front of the experimental system. In addition, a BF_3 counter was used with an active length of only 15 cm instead of the 50 cm of the former counters. In this way the background could be reduced by a factor of about 8.

Owing to these changes the yield of counted spectrum neutrons was of course reduced, but in the meantime the power of the HOR was increased from 500 kW to 2 MW and the coupling between the reactor core and the thermal column was redesigned so that about the same counting rate was obtained compared with the situation before 1968.

Owing to the higher flux level in the thermal column new problems arose since the temperature of the experimental system and the collimators

rose from 20°C up to 60°C during a measurement of, say, 8 hours. The B_4C collimators (70% B_4C, 30% paraffin) had to be mixed with araldite instead of paraffin to safeguard them against melting. A heat exchanger was constructed through which the water from the experimental system is circulated [29]. In this way the temperature in the system could be kept constant within 0.5°C at $\sim$ 20°C.

Comparison of the absolute flux levels in space dependent measurements requires an accurate knowledge of the factor N_m in Eq. (3.1). For the registration of the integrated reactor flux during a measurement, a monitor system has been selected, which produces pulses at a rate proportional to the reactor flux. These pulses can be fed into the PDP 9 in the same way as the pulses from the BF_3 counter, so that any failure of the PDP 9 will act equally on the spectrum counting and the monitor counting. Two fission chambers (diameter $\frac{1}{2}$") have been installed near the chopper (small BF_3 counters are not adequate owing to the high γ flux near the chopper). ^{239}Pu and ^{235}U respectively were used as fissile material in the two counters. Intercomparison of the results of the two counters as well as comparison of measurements of the same spectrum at different rotor speeds showed that the factor N_m in Eq. (3.1) could be determined with an accuracy of about 1%.

In 1969 the spectrometer was coupled to the PDP 9 computer (before that time a TMC multichannel analyser was used as counting system). Up to eight experiments are allowed to run simultaneously on this computer. Counts are added to the core memory by means of a software program. The effect of count losses due to the relatively slow software has been studied (see Sect. 3.2.3.5). The memory contents can be dumped on magnetic tape and used later on for analysis.

The Algol program OWL [30] used for the data reduction has been rewritten in FORTRAN and adapted for magnetic tape input. OWL essentially calculates the neutron spectrum $\Phi(t)$ from Eq. (3.1). A routine for plotting the $E\Phi(E)$ spectrum has been incorporated in OWL. For reduction of the statistics in the plotted spectrum, measured data can be grouped into intervals of equal lethargy and added.

Owing to the modifications of the spectrometer the parameters appearing in Eq. (3.1) had to be reevaluated. The next paragraph deals

with the determination of these parameters.

3.3.3 Analysis of data

3.2.3.1 Calibration of time scale

The clock of the time-of-flight unit is started by the optical system indicated in Fig. 3.1. The rather high temperature near the photocell (due to the high radiation level) causes a reduction of the height of the photocell pulse during a series of measurements. Moreover, the high radiation level causes the lenses in the optical system to become less transparent to the beam of light. In order to make the starting moment of the clock independent of the pulse height, an amplifier has been constructed which differentiates the broad pulse of the photocell and supplies the time-of-flight unit by a short pulse at the moment of zero passage of the differentiated pulse.

It is practically impossible to fix the mirror on the rotor axis exactly parallel to the rotor slit. The moment of zero flight time t_o will therefore not coincide with the starting moment of the time-of-flight unit. Fig. 3.2 shows a measured neutron distribution in which the time-dependent background (Sect. 3.2.3.2) is superimposed on the spectrum neutrons. The mirror was turned about 15^o forward with respect to the rotor slit. Owing to the superposition of spectrum and background neutrons the step in the counting rate of the spectrum neutrons on arrival of the fastest neutrons (at t_o) is completely lost. Moreover, this step is broadened as a result of the final resolution of the spectrometer, and this causes a shift of the peak in the background distribution. Hence, neither the step in the counting rate of the spectrum neutrons nor the peak in the background distribution can be used for the determination of the moment of zero flight time t_o. Therefore, t_o is determined in the following way:

A $2\frac{1}{2}$ cm thick B_4C plate is placed in front of the detector, so that only very fast neutrons (flight times less than 8 μs) are detected. The maximum of the resulting peak indicates the point of zero flight time. This peak could be measured with an accuracy of about one quarter of the

channel width used in the spectrum measurements. As neither a measurement with a 5 cm thick B_4C plate in the neutron beam nor a measurement with a flight path twice as long resulted in a shift of the peak in the counted neutron distribution, it may be concluded that the indication of the zero flight time is correct.

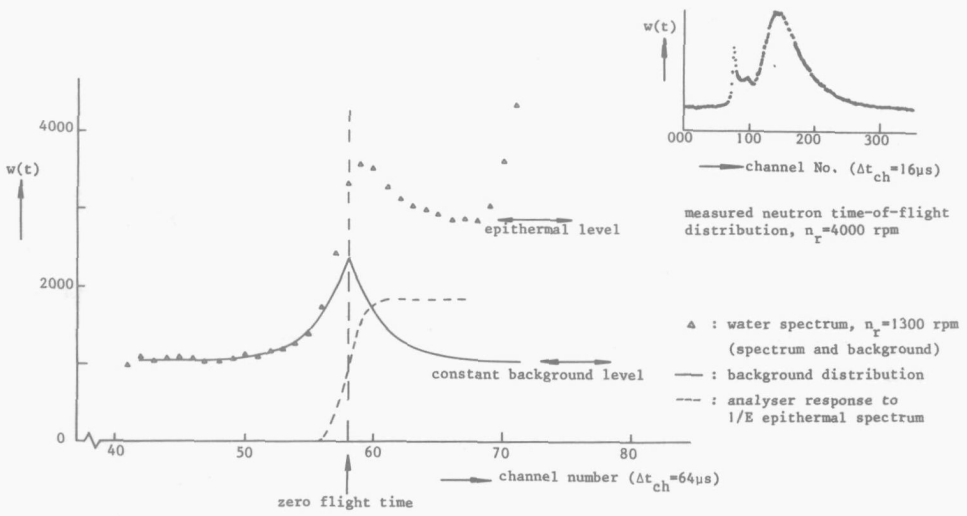

Fig. 3.2 Effect of the time-dependent background and the finite resolution of the spectrometer in the high-energy tail of a time-of-flight spectrum. The peak in the background distribution is caused by fast neutrons transmitted through the rotor. At higher rotor speeds this peak is narrowed, as is shown in the insert (top of the right).

3.2.3.2 Background

In the neutron background two components are distinguishable , viz. a time-dependent part caused by fast neutrons transmitted through the chopper, and a constant part caused by neutrons penetrating the shielding of the experiment (general reactor background) (see Fig. 3.2). The constant background can be determined directly from the memory contents in the last 20% of the channels of the time analyser. In these channels no spectrum neutrons are counted, as the transmission of the

chopper is zero for these slow neutrons (see Sect. 3.2.3.3). The shape of the time-dependent background is indicated by the peak obtained in the calibration of the time scale (Sect. 3.2.3.1). By a proper normalization of this peak the time-dependent background can be determined.

It should be mentioned that the peak of fast neutrons is distorted somewhat by the B_4C plate in the neutron beam. Fortunately this has only a minor effect on the measured spectrum, which fact may be concluded from the following considerations:

- As will be described in Chapter 4, an extraction hole was cut through the experimental system in order to be able to realize the space-dependent measurements. When this hole is filled from the rear with the replaced material to several depths, the space-dependent spectra can be obtained. When the hole is kept empty the measured neutron distribution is simply the total background. Comparison of this background with the distribution obtained with B_4C in the beam showed that the B_4C plate has only a slight broadening effect on the fast neutron peak.
- With a rotor speed above 4000 rpm the resolution of the spectrometer is such that the time-dependent background is confined to neutron energies above 2 eV. Therefore, for comparison with calculated thermal spectra it is hardly necessary to introduce a correction for the time-dependent background.

3.2.3.3 Transmission function

For the time-dependent transmission T of a neutron beam through a rotor (radius r) Larsson [31], and Marseguerra and Pauli [32], have derived an expression under the assumptions that the neutron beam is plane parallel and broad in relation to the slit width, that the rotor axis coincides with the centre of the slit, and that the rotor consists of a material with infinitely large neutron removal cross-section:

$$\begin{aligned} T(\gamma) &= 1 - \frac{8}{3}\gamma^2 \qquad\qquad , \ 0 \leq \gamma \leq \tfrac{1}{4} \\ T(\gamma) &= 8\left(\frac{1}{3}\gamma^2 - \gamma + \frac{2}{3}\gamma^{\frac{1}{2}}\right) , \ \tfrac{1}{4} \leq \gamma \leq 1 \end{aligned} \tag{3.2}$$

with

$$\gamma = \frac{|2\pi n_r t/l_f - 1/2R|}{s/r^2},$$

n_r = rotor velocity,
t = neutron flight time,
l_f = neutron flight path,
R = radius of curvature of the rotor slit,
s = slit width.

The transmission is thus a function of $n_r t$, with l_f, R and s/r^2 as parameters.

In the actual spectrometer the above-mentioned assumptions are not adequate: the neutron beam is not broader than the slit width and the centre of the slit is shifted 17 mm with respect to the rotor axis. Moreover, the cadmium lining of the rotor slit is ineffective for neutrons with energies above 0.5 eV, whereas the removal cross-section of the rotor material is about 1,3 cm^{-1} for energies up to 30 keV. Nevertheless, it is assumed that the formula derived by Larsson can be used provided the values of the parameters R and s/r^2 are adapted in such

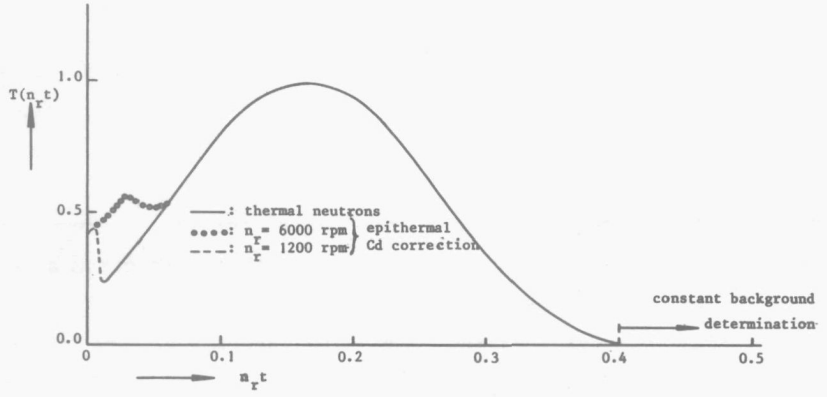

Fig. 3.3 The transmission function of the rotor. Note that $n_r t = 0.5$ corresponds to the arrival of infinitely fast neutrons of the next rotor pulse.

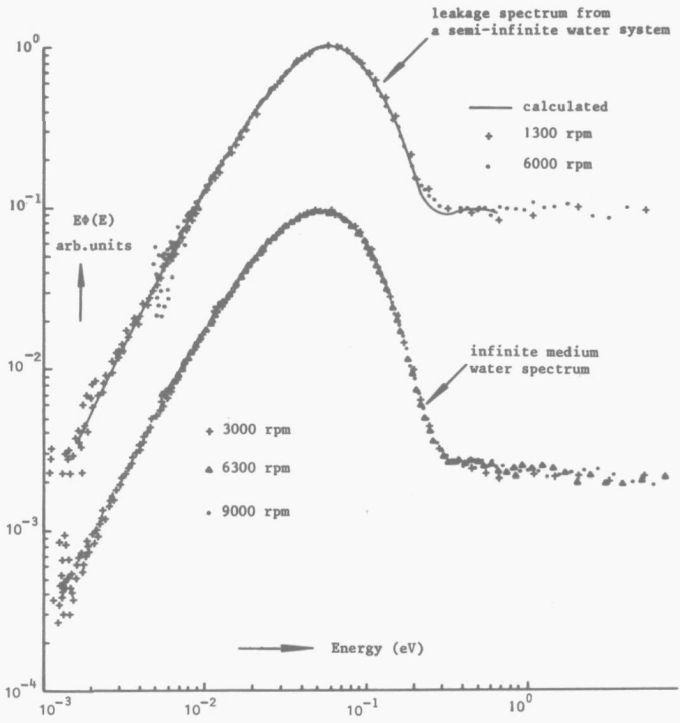

Fig. 3.4 Water spectra measured at different rotor speeds for the experimental determination of the rotor transmission function.

a way that expression (3.2) gives the true transmission function. These "best fit" values were determined experimentally in the following way:

An arbitrary spectrum was measured at different rotor speeds. A "trial-and-error" computer program compared the spectra for various combinations of values for the parameters R and s/r^2 [33]. With this program a combination of values for R and s/r^2 could be obtained for which the spectra coincided fairly well, as they should do. The values obtained for thermal neutron energies are

$$R = 1.59 \text{ m} \quad \text{(design value 1.46 m)}$$

$$s/r^2 = 0.452 \text{ m}^{-1} \quad \text{(design value 0.494 m}^{-1}\text{)}$$

For energies above 0.15 eV the cadmium lining loses its effectiveness and the neutrons will "see" a wider slit. With the same trial-and-error

procedure it was found that the best fit of the spectra was obtained when s/r^2 is taken as $1.36 \times 0.452 = 0.615\ m^{-1}$ for energies above 0.65 eV, whereas between 0.15 eV and 0.65 eV its value is varied in proportion to the variation of the cadmium absorption cross-section.

Fig. 3.3 shows the transmission function of the rotor, determined in the above-mentioned way. Infinite-medium water spectra and leakage spectra from a semi-infinite water medium, measured at different rotor speeds, were analysed with the OWL program using this transmission function. In Fig. 3.4 the coincidence of the measured results is clearly visible.

3.2.3.4 Detector efficiency

The efficiency of the detector is a function of the neutron flight time with the absorption cross-section of the BF_3 gas as parameter (see Fig. 3.5).

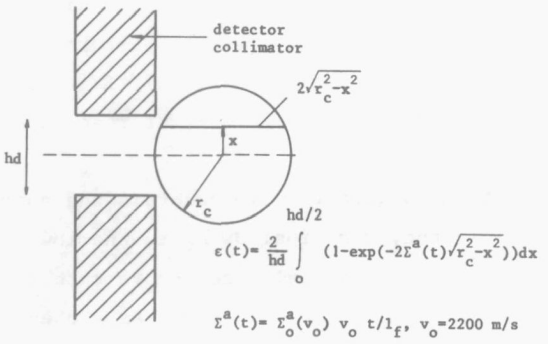

Fig. 3.5 On the derivation of the detector efficiency $\varepsilon(t)$

The absorption cross-section Σ_o^a of the 2" BF_3 counter (type 15 EB 70/50G) had to be determined experimentally, as the manufacturer's data regarding the ^{10}B contents (70 cm Hg gas pressure, ^{10}B enrichment above 90%) were too vague. Therefore, the infinite medium water spectrum was measured with a counter of well-known efficiency, viz. a ½" diameter BF_3 counter filled to a pressure of 40 cm Hg with natural boron. Owing to the small absorption cross-section of this counter its efficiency will vary as the boron cross-section, i.e. in proportion to the neutron

flight time t. The measured spectrum was compared with the water spectrum recorded by the 2" counter. The best fit of the spectra was obtained with a Σ_o^a-value of 0.091 cm^{-1}, corresponding to 90% ^{10}B enrichment.

A few words should be said about the measurement with the ½" detector. It was found that the measured spectrum is sensitive to the position of the detector relative to the axis of the spectrometer; in other words, the spectrum varies in the vertical direction. This can be understood by considering the rotor slit as a diaphragm with a variable vertical aperture proportional to the transmission function T. The mid point of this diaphragm is shifted upwards with increasing neutron energy (see Fig. 3.1): the slowest neutrons are transmitted by the lowermost part of the slit, whilst infinitely fast neutrons are transmitted by the direct-view aperture in the upper half of the slit. Owing to the vertical variation of the neutron spectrum near the detector the efficiency $\varepsilon(t)$ and the transmission T(t) are not fully independent. Consequently the data reduction program OWL had to be adapted to take into account the vertical spectrum variation. The ½" BF_3 counter had to be positioned very accurately, as a misalignment of 2 mm gave a spectrum distortion of 10% or more. As a result of the larger dimensions of the 2" BF_3 counter the effect of the spectrum variation is small for this counter and need not be taken into account.

Fig. 3.6 shows the spectra obtained with the two counters and analysed with the above-mentioned efficiency function. Owing to the low counting rate of the small counter the statistical accuracy is rather poor, although the measurement was continued for one week. As a check on the experimentally determined efficiency function the leakage spectra mentioned in Sect. 3.2.3.3 (which are not perturbed by the probe tube*)) are compared in Fig. 3.4 with the theoretical spectrum obtained with the one-dimensional transport theory computer program THERMOSLAB III which takes into account anisotropic scattering [34]. From Fig. 3.4 it can be seen that the theoretical and experimental results are in close agreement.

---

* See also the foot-note on page 52.

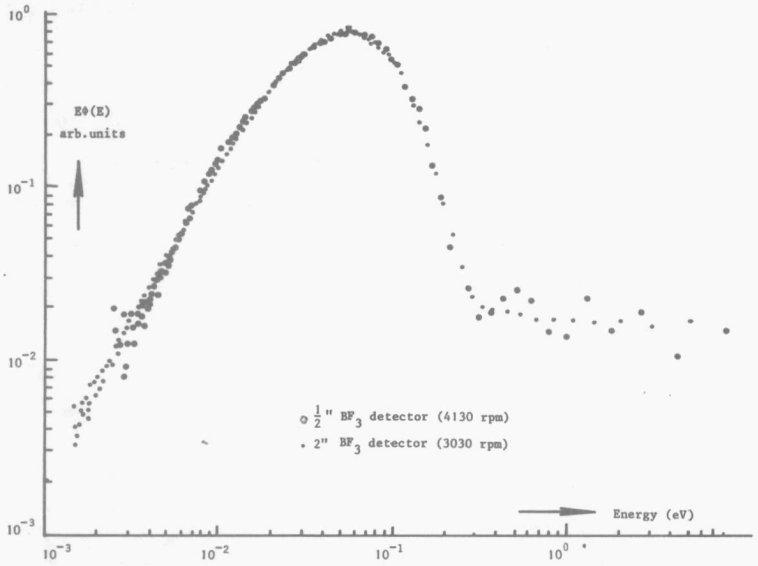

Fig. 3.6 Infinite-medium water spectra obtained with two detectors.

3.2.3.5 Other corrections

In the factor g(t) in Eq. (3.1) one can distinguish (a) the effect of count losses in the counting system, (b) the transmission through materials present in the neutron beam, and (c) the spectrum distortion due to the time resolution of the spectrometer.

(a) The maximum counting rate obtainable with the spectrometer is about 1850 counts per second when the infinite-medium water spectrum is measured. The counting rate for the spectra described in Chapter 4 is generally lower than 300 counts per second. Count losses in the BF_3 detector (dead time $\sim$ 5 μs) are thus neglegibly small (<0.5% for count rates of less than 1000 counts per second). The dead time of the TOF unit (manufacturer Laben) is 2 μs. The TOF unit has two buffers for temporary storage of counted neutrons. The PDP 9 data-counting routine has a running time δ of about 50 μs, which was verified experimentally with a pulse generator. δ can be divided into δ_1 = 18 μs for searching the experiment which offers data, and δ_2 = 32 μs, needed for data storage. The effect of the two buffers in

the TOF unit was examined with a γ source/detector system which provided the PDP 9 with a variable number of counts per second. Table 3.1 shows some results from which it may be concluded that any spectrum distortion due to count losses will be well below 0.5%. Moreover, high counting rates of other experiments which run simultaneously will have no effect on the measured absolute flux level, since the distortion due to other experiments will be equal for the spectrum counting rate and the monitor counting rate.

n (c/s)	n'/n
20000	0.760
10000	0.897
6000	0.979
2940	0.987
1100	0.998

Table 3.1
Count losses in the time analyser.
n is the "input" counting rate.
n' is the "output" counting rate.

(b) The spectrum distortion due to neutrons removed from the neutron beam by scattering and absorption in the aluminium windows of the evacuated flight tube and chopper house, in the copper lining of the BF_3 counters and in the air between experimental system and chopper, was calculated to be within 2% [8].

(c) The resolution of the spectrometer is determined by the rotor pulse width, the analyser channel width, the time for a neutron to pass through the detector and the time for the rotor-slit axis to scan the source surface. The finite rotor pulse gives by far the largest contribution to the finite resolution of the spectrometer(full width at half-height of the rotor pulse $\underset{\sim}{}$ 50 μs for a rotor speed of 4500 rpm). It is possible to calculate a correction for the resolution of the experiment [35]. Neglecting higher derivatives of the observed time spectrum $n_{obs}(t)$ than the second order, the true spectrum n(t) is given by

$$n(t) = n_{obs}(t) - \frac{1}{2}\frac{d^2 n_{obs}(t)}{dt^2}\int_{-\infty}^{\infty} t'^2\, r(t')dt', \qquad (3.3)$$

where r(t') is the resolution function.

For a pure Maxwell spectrum the distortion is found to be below 1%. For the measurements described in this thesis the maximum distortion occurs in the joining region around 0.25 eV between thermal and epithermal energies.

In the data reduction program OWL the factor g(t) (ref. Eq. (3.1)) is set equal to 1. Comparison of the measured and the calculated leakage spectrum in Fig. 3.4 justifies this approximation. Except for the joining region, in which the resolution causes a perturbation of about 3%, the agreement between measurement and calculation is very good. Some spectra described in Chapter 4 show a resonance structure. Owing to this resonance structure the resolution causes a spectrum distortion of up to 15%. As the statistical accuracy of these measurements is rather small it is not useful in the OWL program to derive the second derivative $\frac{d^2n(t)}{dt^2}$ from the measured data. Where the resolution has a noticeable effect, this will be indicated in Chapter 4.

3.2.4 Accuracy of measured spectra

In the figures of Chapter 4, in which $E\Phi(E)$ spectra are shown, the estimated errors in the energy E and the $E\Phi(E)$-values of the measured data are indicated by error margins. The maximum error ΔE in E is determined by the accuracy with which the time calibration can be performed. In Sect. 3.2.3.1 it has been pointed out that the time uncertainty is about one quarter of the analyser channel width. The relative error in $E\Phi(E)$ is equal to the sum of the relative errors in the factors appearing in Eq. (3.1). The accuracy of the monitor system as well as the determination of the background is about 1%. The accuracy of the transmission function and the detector efficiency may be estimated from the accuracy with which the measured spectra in Fig. 3.4 and Fig. 3.6 coincide. From comparison of the measured and the calculated results in Fig. 3.4 it may be concluded that the maximum error caused by T(t),

$\varepsilon(t)$, $g(t)$ and $b(t)$ is about 3% for thermal energies and about 5% for energies above 0.2 eV, provided the effect of the resolution of the spectrometer is evaluated correctly (the effect of a 1% error in $b(t)$ depends, of course, on the ratio of $w(t)$ and $b(t)$). The error in $w(t)$ is purely statistical.

3.3 ACTIVATION TECHNIQUES

3.3.1 General considerations

The activation measurements described in this thesis may be divided into:

(a) spectrum index measurements by means of activating Lu and Dy foils;
(b) neutron density measurements by means of activating small Dy pins.

The spectrum index SI is defined as

$$SI = \left(\frac{^{177}\text{Lu activity}}{^{165}\text{Dy activity}} \right)_{\substack{\text{unknown} \\ \text{spectrum}}} \Big/ \left(\frac{^{177}\text{Lu activity}}{^{165}\text{Dy activity}} \right)_{\substack{\text{known} \\ \text{spectrum}}} \qquad (3.4)$$

The "known spectrum" is the infinite-medium water spectrum shown in Fig. 3.4. A pair of foils is irradiated in the known spectrum simultaneously with the irradiation of foil pairs in the experimental system. The foils have a thickness of 0.125 mm and a diameter of 6 mm. They consist of an aluminium alloy, containing, respectively, 4.9% Dy and 5% Lu.

The method of pin measurements is due to Tas [38]. In a review paper [39] Stamm'ler showed that with this method very accurate and reliable results can be obtained. It was therefore included in the experimental program. The Dy pins are 8 mm long and have a diameter of 0.75 mm or 0.38 mm. They consist of a 10% Dy-90% Al alloy.

3.3.2 Analysis of data

Although the activation technique is fairly simple, correct interpretation of the results obtained calls for accurate evaluation of the perturbations and inaccuracies inherent in the measuring technique [39,40].

A short review of this evaluation will be given here.

(1) Flux distortion due to insertion of the activation detectors and other construction materials.

The absorber rods shown in Fig. 3.7 were used for the positioning of the foils and pins. In the moderator a 8 mm thick perspex holder was provided. The foils were affixed to these holders with waterproof scotch tape. For the positioning of the pins, holes were drilled in the perspex.

The effect of the insertion of Dy pins was evaluated experimentally by using pins of different diameter, viz. 0.75 mm and 0.38 mm, in holes with a diameter of, respectively, 0.8 mm and 0.4 mm. By way of illustration, Fig. 3.8 shows the Dy-activity across a system, already described in Sect. 2.5, Fig. 2.12 (further details of the experimental system are given in Chapter 4). Linear extrapolation to unperturbed Dy-activity shows that a maximum error of 2.6% occurs for 0.38 mm diameter pins. The error caused by linear extrapolation (of the volume of the pins) is estimated at less than 0.5%. In Fig. 3.8 the activity of the Dy foils is also shown. The per-

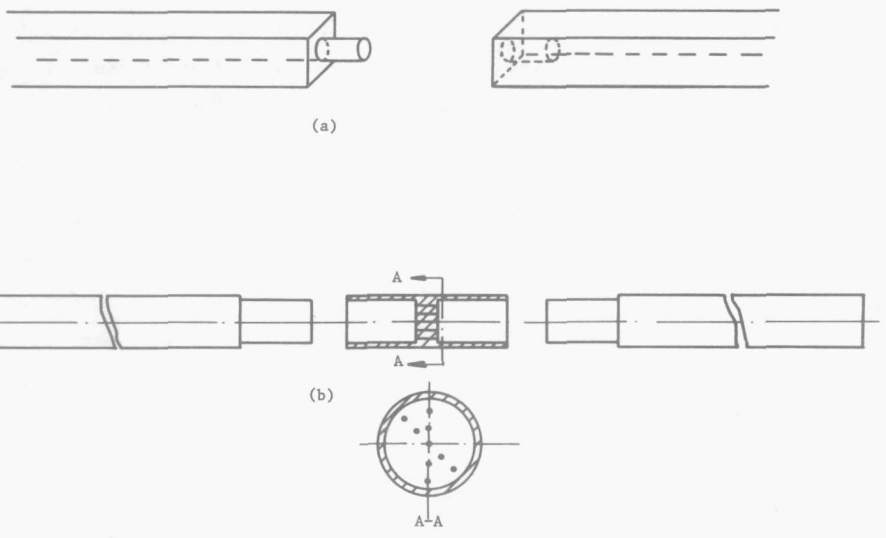

Fig. 3.7 Iron rods used for foil measurements (a) and pin measurements (b). For the foils a hole of 6 mm diameter was drilled; the holes for the pins have a diameter of 0.4 mm or 0.8 mm.

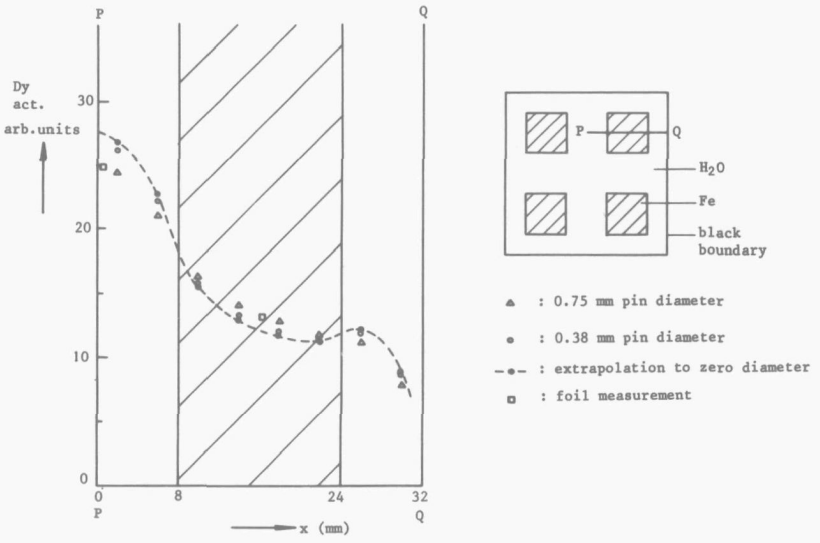

Fig. 3.8 Dy activity measured with various detectors.

turbation caused by the foils is clearly rather large. Nevertheless, no correction was made in the spectrum index (SI) values, as a flux distortion will act on both the Lu and the Dy activity. Multigroup calculations in one-dimensional slab geometry showed that the error in SI in systems in which the Dy activity is perturbed by 8%, is less than 2%.

The flux distortion due to the perspex was not evaluated, since perspex closely simulates water [39]. However, an effect of 1% in the spectrum index and the Dy activity may still be expected. The flux distortion caused by streaming of neutrons through gaps for the positioning of the detectors was eliminated by the special construction of the rods.

(2) Inaccurate positioning of the detectors.

The precision fabrication of the rods provides for very accurate positioning of the detectors. The same applies to the positioning of the pins in the moderator. It should be mentioned here that the perturbation caused by the relatively thick perspex holder will be much smaller than the error caused by possible mispositioning

when a less rigid pin holder is used.

Inaccurate positioning of the foils in the moderator gives rise to a maximum estimated error of 0.5% in the spectrum index.

(3) Activation by epithermal neutrons.

The activity induced by epithermal neutrons can in principle be evaluated experimentally by sub-cadmium measurements. As a cadmium cover would cause a large flux perturbation in the present measurements, no correction was made for the epithermal neutron activation; when measurements are compared with calculations this activation is accounted for in the calculations. Owing to the small resonance integrals of Lu and Dy as compared with the thermal cross-sections, the epithermal contribution to the activation is in any case small.

(4) Temperature variation during irradiation.

During irradiation the heat exchanger employed in the time-of-flight measurements was not used, since the activation times were rather short. Nevertheless, a temperature rise of 5 ^{o}C was observed in spectrum index measurements, whilst in a few pin measurements a rise of 15 ^{o}C occurred. Since the temperature rise is equal for the unknown spectrum and the reference spectrum, the associated error in the spectrum index is a second-order deviation. Calculations showed that the error in SI is well below 1% , whilst a temperature shift of 20^{o}C perturbs the shape of the spatial neutron density distribution by not more than 1%.

(5) Inaccuracies of the counting system.

The γ activity of each detector was counted with a NaI scintillation counter. The β activity was shielded by a perspex holder in which the detector was placed. As β radiation is partly shielded by the detector material, the error in the β counting rate caused by possible variations in the thickness of the detectors was thus eliminated. The scintillation counter was calibrated continually with a ^{57}Co and a ^{241}Am γ source. An automatic detector changer was constructed in which the detector holder could be positioned accurately with respect to the NaI counter. From Eq. (3.4) it can be observed that any difference in the counting efficiency for the γ photons of Lu and Dy is eliminated in the SI value. Before and after being counted the detectors were kept in lead containers (see Fig. 3.9).

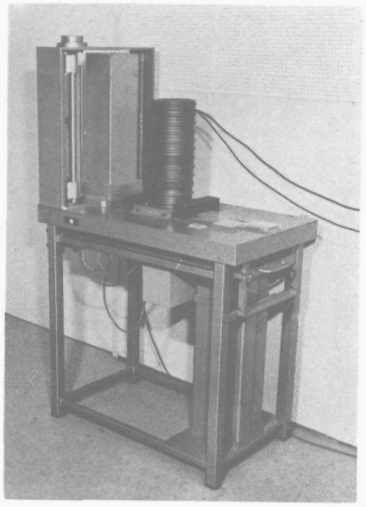

Fig. 3.9 Automatic detector changer with lead containers for detectors to be counted (left), scintillation counter (middle) and counted detectors (right).

(6) Correction for decay of activity.

The observed activity of the detector was corrected for decay after irradiation and during counting with the aid of a second counting system in which a reference detector of similar composition, irradiated simultaneously, was counted during the same time. Thanks to this method of compensation, accurate knowledge of the half-lives of the isotopes was not necessary.

(7) Inhomogeneous composition of the alloys.

It was found that differences in the counting rate of foils and pins of the same weight, irradiated in the same flux, were as great as 10%. Therefore, the detectors had to be calibrated. After the decay of activity the detectors were placed on a rotating disk, irradiated in an arbitrary spectrum and counted again.

Activation analysis showed that the amount of impurities in the detector materials was neglegibly small.

(8) Statistical accuracy.

The statistical error varies for each detector. This error is a function of the number of counted photons from the detector, the compensation detector and the background. For calibration of the detector the same consideration applies. The total statistical inaccuracy was generally about 1%.

3.3.3 Accuracy of the measured activation

In Sect. 3.3.2 the errors in the actual activation measurements were summarized. It is found that the flux depression caused by the detectors is the major source of inaccuracy in the foil measurements, whilst the effect of the perspex holder in the moderator leaves an uncertainty of about 1% in both foil and pin measurements. When measurements are compared with calculations the effect of a temperature rise can be taken into account in the calculations. The total uncertainty in the spectrum index and the Dy pin activity is estimated to be 4% and 2.5%, respectively. In regard to accuracies, the activation method is thus able to compete with the time-of-flight method (ref. Sect. 3.2.4), but the energy resolution of time-of-flight measurements is of course much better.

4. COMPARISON BETWEEN CALCULATIONS AND MEASUREMENTS

4.1 GENERAL CONSIDERATIONS

Although it was argued in Chapter 2 that one may expect reliable results from THERMOGENE, the ultimate test of its reliability should be furnished by comparison with experiments. In Sect. 2.5 several aspects were summarized which can be distinguished when computation results have to be verified. From these aspects the following should be considered when a comparison with measurements is carried out:

(a) The basic data. Since this investigation aims primarily at verification of a calculation model, the basic data of the materials used in experiments should be well known. On the other hand one may say that these materials need not be realistic reactor materials provided their cross-sections are similar to the cross-sections of the materials used in a reactor. From this point of view it is fully justified that uranium has been simulated by iron in order to avoid high activation levels.

(b) The scattering models for the moderating materials. The models used in this research have proved adequate for well-thermalized spectra and for regular lattices [8,10,19]. However, verification of their adequacy in heavily undermoderated systems (as in modern light water reactors) or in systems with materials exhibiting a resonance structure in their cross-sections (as in plutonium-recycled reactors) still seems to be necessary.

(c) The numerical approximation to the transport equation. The effect of spatial discretization could be examined without experimental

verification (Sect. 2.4). As regards the number of energy steps and the thermal cut-off energy, a verification for spectra with a resonance structure remains, however, necessary. The isotropic scattering assumption proved to be inadequate in the presence of heavily absorbing materials by comparison with the linear anisotropic scattering approximation. The adequacy of this latter approximation should thus be verified by comparison with still better approximations or with experiments.

For the experimental verification of THERMOGENE the experimental systems have to be selected very cauteously. The following considerations should be observed:

(a) The experimental system should have a two-dimensional x-y geometry. The dimensions of the system are limited, however, by the dimensions of the thermal column. All the experiments were carried out in a water container of 25 x 25 x 25 cm (Fig. 4.1). The buckling in this container is about $-0.05\ cm^{-2}$, which may be concluded from a comparison of the "infinite-medium" water spectrum measured in the centre of this container (see Sect. 3.2.3.3, Fig. 3.4) with an infinite-medium calculation; the best concordance with the experimental data is obtained when a buckling of $-0.05\ cm^{-2}$ is assumed in the calculation (the buckling in a true infinitely large system is zero). Foil measurements showed that the buckling in the z direction, which is the direction from the reactor core to the experimental system, is $-0.037\ cm^{-2}$ [8]. In order to minimize the effect of buckling on the measured spectra, the neutron leakage in the x and y directions, which is treated correctly in the calculations, should be made very large. This has been achieved by surrounding the experimental x-y system in the centre of the container by a 0.5 mm thick cadmium cylinder. The buckling B^2 in the z direction can be taken into account by means of a correction based on diffusion theory, viz. by replacing $\Sigma^a(E)$ by $\Sigma^a(E) + D(E)B^2$, where D(E) is the energy-dependent diffusion coefficient. Calculations showed that the effect of the finite dimensions of the water container is less than 1% for the spectra to be described in this chapter, so that a possibly

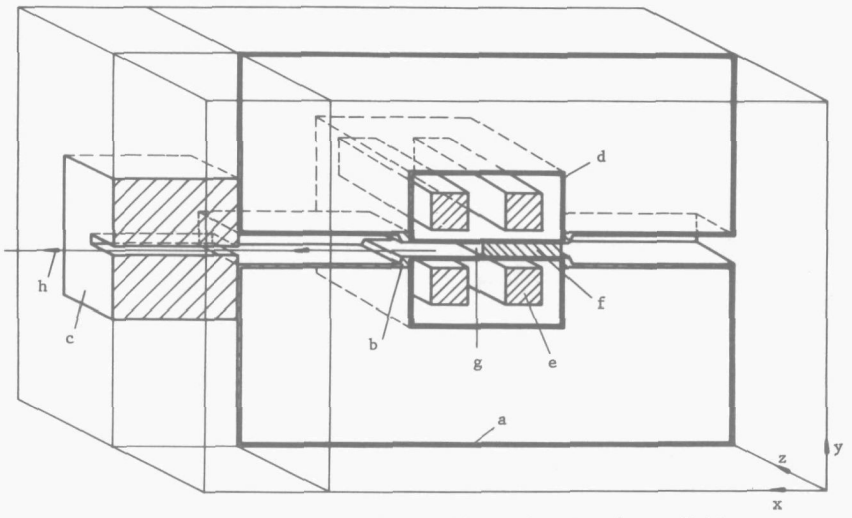

Fig. 4.1 Schematic three-dimensional view of the experimental system.
a - water container (25x25x25 cm); b - probe tube (Y-Z cross-section in the centre of the container 6x90 mm); c - collimator (4x50 mm); d - Cd cylinder (X-Y cross-section 64x64 mm); e - Fe rod (16x16 mm); f - CH_2 plate; g - source area; h - neutron beam.

incorrect prediction of the effect can safely be neglected*).

(b) The experimental system should provide a thorough check on the predicted spectra. Large flux gradients should be present and, if possible, the spectra should show a resonance structure. This has been achieved, inter alia, by the use of fairly thick rods, viz. square rods of 16 x 16 mm^2 and 15 mm diameter circular rods. The above-mentioned cadmium cylinder, which has a square cross-section, simulates a crucifix-shaped control rod and causes also a steep flux depression. In a series of measurements the circular rods were covered with a 0.03 mm thick layer of cadmium. Owing to the resonance in the absorption cross-section of cadmium near 0.18 eV a simulation of ^{239}Pu, bred in uranium rods, could be accomplished.

* The "semi-infinite medium" leakage spectrum mentioned in Sect. 3.2.3, Fig. 3.4, is the spectrum emerging from the wall of the container in the direction of the BF_3 detector. A probe tube penetrating into the container need not be used. The effect of buckling on this leakage spectrum proved to be less than 2%.

(c) The perturbation caused by the extraction channel (probe tube) used in time-of-flight measurements should be evaluated correctly. The low count rate in the present measurements prevented the choice of a small probe tube, which would not disturb the spectra. In agreement with an examination carried out by Caspers and Janssen [11] a probe tube was chosen having a rectangular cross-section with one side (in the z-direction) much longer than the other side (in the y-direction). The position of the bottom of the probe tube was varied so that space-dependent (x-dependent) spectra could be measured. The probe tube consists of 1 mm thick aluminium, the inner dimensions are 90 x 6 mm. Variation of the z dimension of the probe tube from 60 mm to 100 mm had a neglegible effect on the measured spectra so that the z dimension of the probe tube may be considered in the calculations as infinitely long. The experimental system may thus be considered still to have x-y geometry, and the effect of the probe tube can be evaluated correctly in the calculations.

It should be remarked here that *angular* spectra have been measured with the time-of-flight spectrometer. Scalar spectrum measurements, which can be performed with a zirconium scatterer, are adversely affected by the fact that the neutron counting rate is lower. Moreover, angular spectra are more sensitive to geometrical details of the system and hence to the calculation model to be verified.

(d) The present verification relates to thermal spectra; therefore, the epithermal neutron spectrum should be as simple as possible, i.e. space-independent and with a 1/E energy dependence. For that reason cadmium was chosen for simulation of the crucifix-shaped control rods since boron also acts upon the epithermal neutrons. Gold foil measurements indicated that the epithermal flux in the systems to be described in this chapter may be considered to be space-independent [8]. The source term in the calculations could thus be treated as isotropic and space-independent (ref. Eq. (2.4)). In the calculations the cadmium cylinder was considered as a black boundary for neutrons with energies below 0.63 eV, whilst above this energy the absorption of the cadmium was neglected. It should be mentioned that this assumption is not quite correct, as the cadmium cylinder becomes "grey" for neutrons with energies above 0.2 eV. One-dimensional

slab calculations in which a cadmium plate was taken into account correctly, showed that the scalar spectra close to the cadmium are underpredicted by about 12% between 0.25 eV and 0.63 eV. The effect of the approximate treatment of the cadmium on the predicted detector activations is, however, less than 1%, as these quantities are integrated over all energies. The effect on the predicted *angular* spectra near the cadmium is also neglegibly small: the effect on the scalar spectra is confined to locations at a distance of less than 1 cm from the cadmium, whilst the angular flux in the energy region between 0.25 eV and 0.63 eV is made up of neutrons born (i.e. scattered from *all* energies into this energy region) at locations up to several centimeters from the cadmium.

Before turning to the actual measurements and calculations a few observations may be made in order to facilitate the present survey. The systems in which spectra have been determined are numbered, so that reference can be made to each particular spectrum, Dy activity profile or spectrum index distribution.

All the spectrum measurements were carried out at room temperature ($20^{\circ}C$), whilst in the activation measurements the temperature was generally $25^{\circ}C$ to $30^{\circ}C$.

In all the spectrum measurements the rotor speed of the chopper was 4000 rpm*). This rotor speed was selected as a compromise between low speeds in order to obtain a low cut-off energy of the transmission function and high speeds entailing good resolution of the spectrometer. The time analyser channel width was 16 μs.

In the calculations to be verified use was made of the conclusions drawn in Chapter 2 with regard to the accuracy of predicted quantities. Hence, time-of-flight measurements are compared with calculations based upon linear anisotropic scattering and the flat-flux approximation (exceptions to this rule will be indicated where necessary). Activation

---

* For the determination of the transmission function (Sect. 3.2.3.3) several rotor speeds between 1300 rpm and 9000 rpm were selected. For the determination of the efficiency function (Sect. 3.2.3.4) the rotor speed was 4130 rpm.

measurements are compared with calculations based upon the isotropic scattering approximation; the calculated distributions shown in this chapter were obtained by averaging the values calculated with the two transport models described in Chapter 2: the flat-flux approximation and the point-flux approximation. The number of energy groups in the calculations was 10 when water was the only moderator in the experimental system, and 21 when polyethene was present (see page 18).

Each group of measured spectra shown in one figure was normalized to the external monitor described in Sect. 3.2.2; the calculated spectra were normalized with respect to the source term, i.e. to the epithermal 1/E spectrum. The group of measured spectra was then normalized to the calculated spectra in such a way that the best possible matching was obtained.

4.2 SYSTEMS WITH SQUARE RODS

In this section space-dependent spectra are shown which were obtained from systems with square rods. A square section of the rods was selected to provide an accurate description of the position of the source area, i.e. the bottom of the probe tube. Fig. 4.1 shows a three-dimensional view of the experimental system. An extraction channel extending to both sides of the water container was inserted. Fig. 4.2 shows an extraction channel with a 9-rod system built up around it. Measurements with an empty channel provided a good check on the alignment of the spectrometer*), whilst the neutron background distribution could also be obtained. Outside the cadmium cylinder of the experimental system the probe tube was covered with 0.5 mm thick cadmium to prevent thermal neutrons from streaming into the cylinder via the extraction channel. For the spectrum measurements the material displaced by the probe tube was inserted again from right to left. If water had to be replaced it was simulated by polyethene plates. The iron rods could be

---

* The spectrometer was aligned optically with a theodolite every time when the experimental system in the water container was modified.

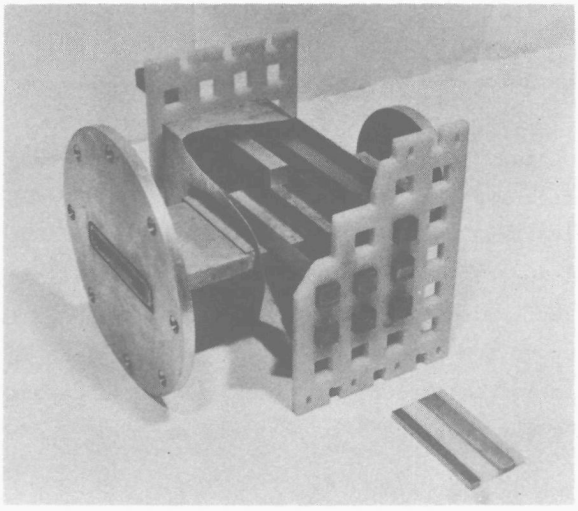

Fig. 4.2 Cut-away view of system No. 3, containing 9 Fe rods, built up around the extraction channel. In front some insert pieces are shown.

positioned precisely by means of two polyethene grid plates at both ends of the rods.

Figs. 4.3 and 4.4 show the spectra obtained from systems 1, 2 and 3, containing respectively 4, 1 and 9 iron rods. The two measured spectra of systems 1 and 2 were normalized to each other on the epithermal flux above 1 eV, since the monitor system had not yet been installed during these measurements. The spectra of the 9-rod system were correctly normalized with the monitor system.

In the calculations *isotropic* scattering was assumed. Each system was divided into square regions of 4 x 4 mm^2. For the 9-rod system polyethene was not taken into account; this was done to limit the calculation time because of the large number of regions, viz. 288, for which spectra had to be calculated.

From Figs. 4.3 and 4.4 the following conclusions may be drawn: Calculated spectra in systems 1 and 2 are in agreement with the measurements within the experimental error. The spectra inside system 3 (positions 2 to 5) are also correctly predicted. The small amount of polyethene present in this system and the fact that the spectra were fairly well thermalized, thanks to the large moderator/absorber volume ratio M/A = 3, are the reasons why the incorrect representation of polyethene in the

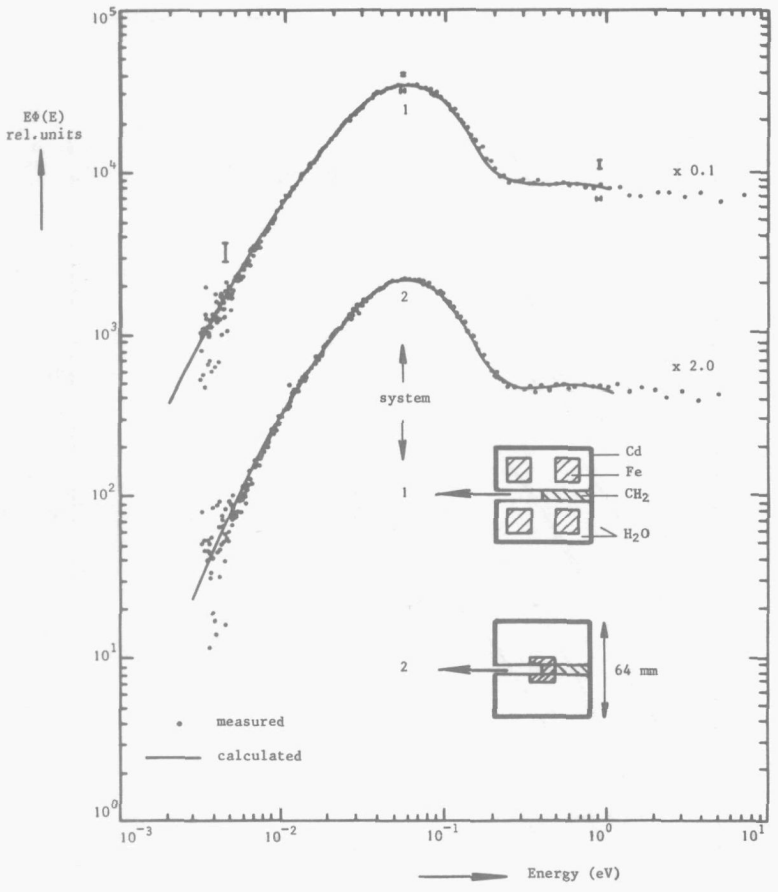

Fig. 4.3 Angular spectra from systems 1 and 2.

calculations is no serious drawback (well-thermalized spectra tend to a Maxwellian distribution irrespective of the used scattering model). Calculations showed that the amount of polyethene present in system 1 has a noticeable effect; for this system polyethene had to be correctly taken into account. The isotropic scattering approximation in all the calculations gives clearly a correct prediction of the spectra inside the systems since the flux gradients are relatively small. Owing to the large flux gradient near the boundary of system No. 3 the isotropic scattering approximation fails to predict the leakage spectrum at the boundary (position 1) (cf. the calculated leakage spectra shown in Fig. 2.14, page 26).

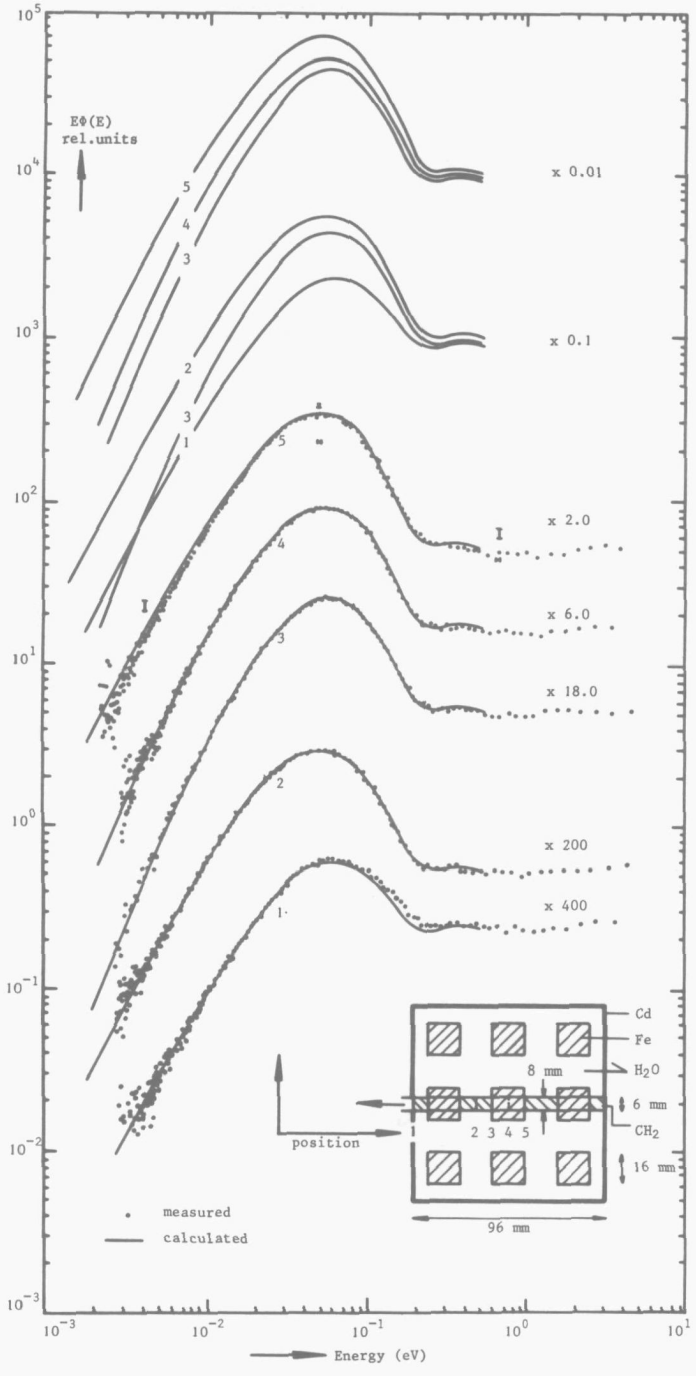

Fig. 4.4 Angular spectra from system 3.

In Figs. 4.5 and 4.6 the spectrum index and the Dy activity are shown for systems 1 and 3. In the activation measurements the probe tube was, of course, not present. Figs. 4.5 and 4.6 show good agreement between measurement and calculation. The differences in the measured data for symmetrical positions indicate that the error caused by statistics and by mispositioning of the detectors is very small. It should be remembered that the spectrum index is an activation ratio normalized to the ratio in a reference spectrum. This normalized ratio has been determined experimentally and theoretically; normalization of the calculated distributions to the measured data in order to obtain a "best fit" has been omitted.

Summarizing, it may be concluded that THERMOGENE gives a correct prediction of the space and energy distribution of the neutron flux, provided anisotropic scattering is accounted for near black absorber blades. The spatial discretization applied in THERMOGENE (4 x 4 mm^2 regions) is clearly sufficient for systems with comparatively thick

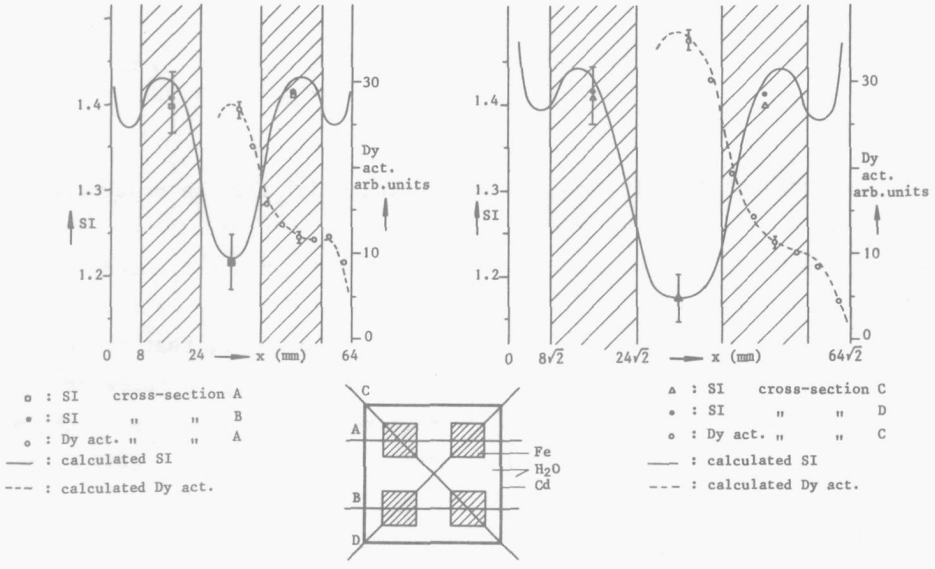

Fig. 4.5 Spectrum index (foil measurements) and Dy activity (extrapolated to zero pin diameter) in system 1.

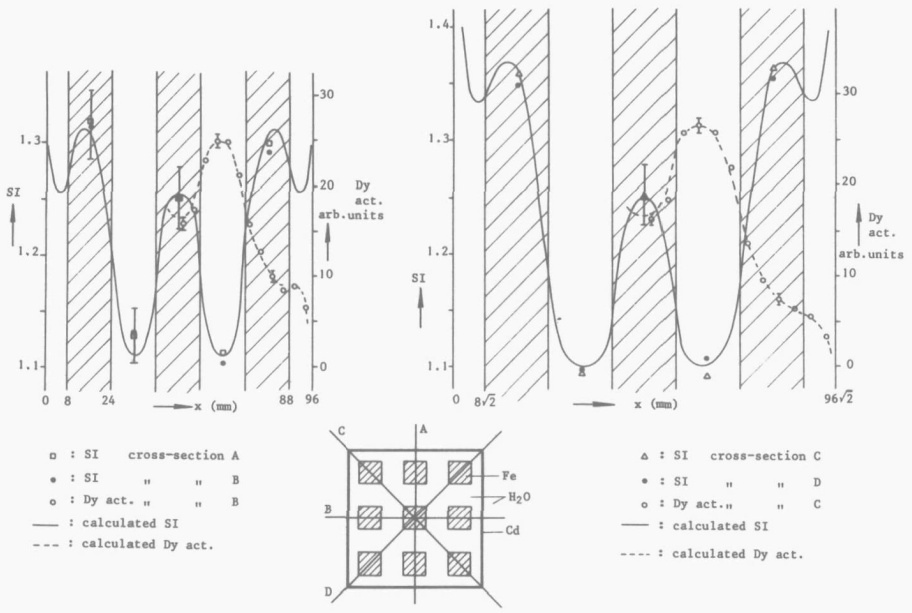

Fig. 4.6 Spectrum index (foil measurements) and Dy activity (extrapolated to zero pin diameter) in system 3.

absorber rods of 16 x 16 mm^2. The scattering model for the moderators (Koppel-Young for H_2O and Goldman for CH_2) and the number of energy groups (10 groups for H_2O and 21 for CH_2) give a correct prediction of the energy dependence of the flux for the fairly well thermalized spectra of systems 1, 2 and 3. It should be stated, however, that the good agreement between theory and experiment in Fig. 4.4 may be somewhat flattering: the error due to the incorrect representation of polyethene in system 3 may have cancelled to a certain extent the error caused by the flat-flux approximation. The effect of polyethene replacing water will be brought up again in the next section.

The spatial resolution of the spectrometer obtainable with the probe tube used in these measurements is satisfactory. The spectral shift across the central rod of system 3 can be measured quite well.

The difference between the incoming and the outgoing flux of the central rod (positions 3 and 5 in Fig. 4.4, where the scalar spectra are equal) shows that the measurement of angular spectra provides a thorough check of the calculation model.

4.3 SYSTEMS WITH CIRCULAR RODS

In the foregoing section no use has been made of the possibilities of THERMOGENE in regard to its description of complex geometries. In this section more realistic models of reactor lattices are considered, viz. square box cells containing circular rods with a smaller moderator/absorber volume ratio.

Fig. 4.7 shows the Dy activity distribution in systems 4 and 5, containing nine rods, with a moderator/absorber volume ratio of, respectively, 1.0 and 2.0. The small dimensions of these systems allowed a very fine spatial discretization in the calculations (114 flat-flux regions in each octant of the systems).
The flux peaking factor F, defined as

$$F = \frac{\Phi_{max}}{\bar{\Phi}}$$

where

Φ_{max} = flux in the central absorber rod where the highest flux occurs,
$\bar{\Phi}$ = average flux in the nine rods,

was predicted correctly by the calculations (F= 1.36 and 1.53 respectively for system 4 and 5). The slight deviations between calculation and experiment are clearly systematic. They may have been caused by incorrect extrapolation to zero pin diameter. The low thermal flux in systems 4 and 5 does not prevent accurate measurement of the Dy activity (compare $\Phi_{thermal} / \Phi_{epithermal} \simeq 60$ for the infinite-medium water spectrum with $\Phi_{thermal} / \Phi_{epithermal} \simeq 4$ for the central absorber rod of system No 4).

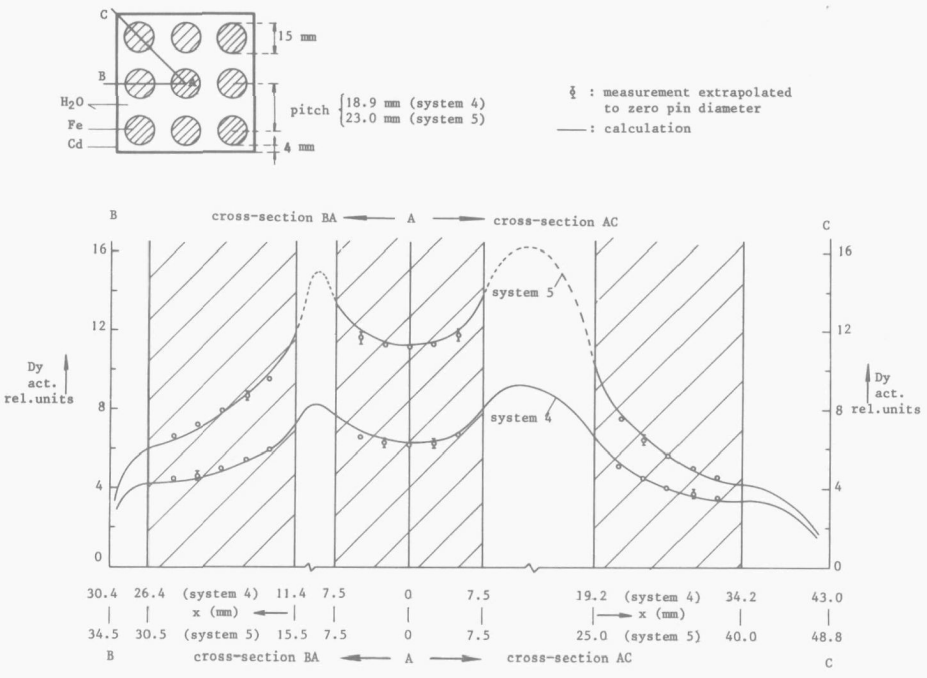

Fig. 4.7 Dy activity in systems 4 and 5.

Fig. 4.8 shows the Dy activity in system 6, containing 25 iron rods and with a moderator/absorber volume ratio of 1.08. The agreement between theory and experiment is satisfactory. The isotropic scattering approximation applied in the calculation is clearly sufficiently accurate to predict reaction rates correctly within a few per cent in this fairly realistic model of a BWR box cell. The calculated variation of the Dy activity over the system is somewhat greater than the measured variation. This may be due to the procedure followed in the evaluation of the effect of spatial discretization (averaging of the distributions obtained with the flat-flux and the point-flux approximation). Incorrect extrapolation to zero pin diameter in the measurement may also have contributed to the deviations.

From system 6 leakage spectra were measured at two positions. They are shown in Fig. 4.9. As no spectra inside the system were measured, a probe tube was used which did not penetrate into the system (see Fig. 4.10). The bottom of the aluminium probe tube was 0.5 mm thick. The procedure for the check on the alignment of the spectrometer employed for systems 1, 2 and 3 could not be used with this probe tube. Therefore, a 1 cm thick CH_2 frame with a vertical opening of 6 mm was mounted on the top of the probe tube before the iron rods were inserted in the water container (Fig. 4.11). A measurement without water in the

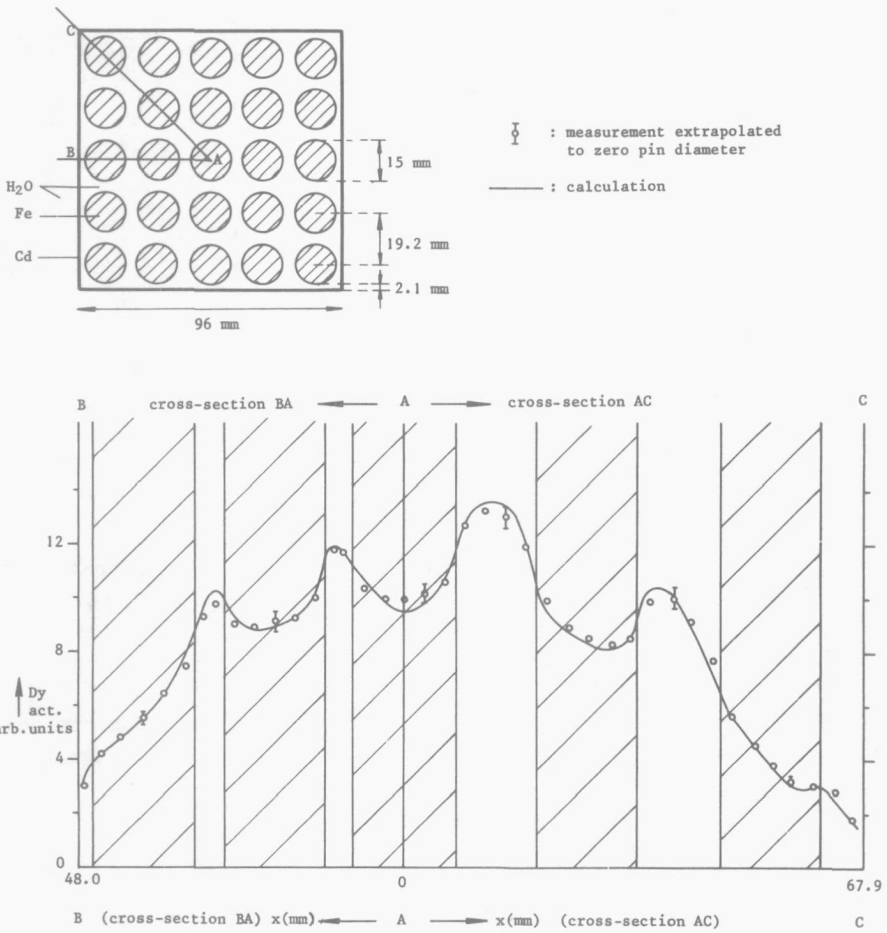

Fig. 4.8 Dy activity in system 6.

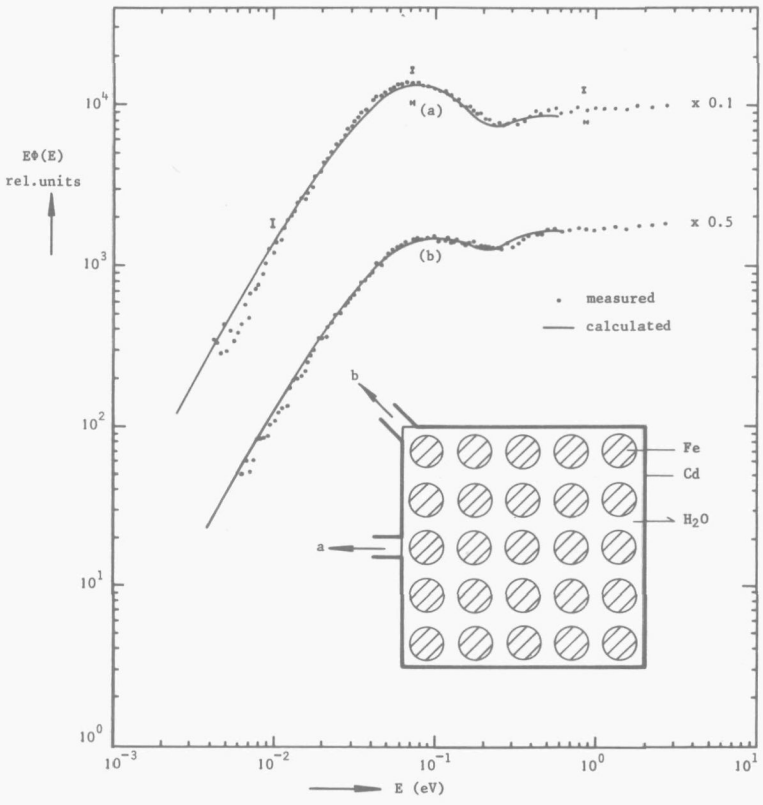

Fig. 4.9 Angular spectra from system 6.

container provided a good check on the alignment, since a thermal spectrum would have been observed if the detector could have seen the CH_2 walls.

The leakage spectra shown in Fig. 4.9 provide a good check on the calculation since anisotropic scattering effects become important near the black boundary of the system. In the calculation the system was divided into 75 flat-flux regions per octant; linear anisotropic scattering was assumed.

Measurements and calculations agree within the experimental error. The slight deviations around 0.05 eV and below 0.01 eV may be due to the flat-flux approximation in the spatial discretization applied in THERMOGENE (cf. the calculated angular spectra shown in Fig. 2.11, page 24).

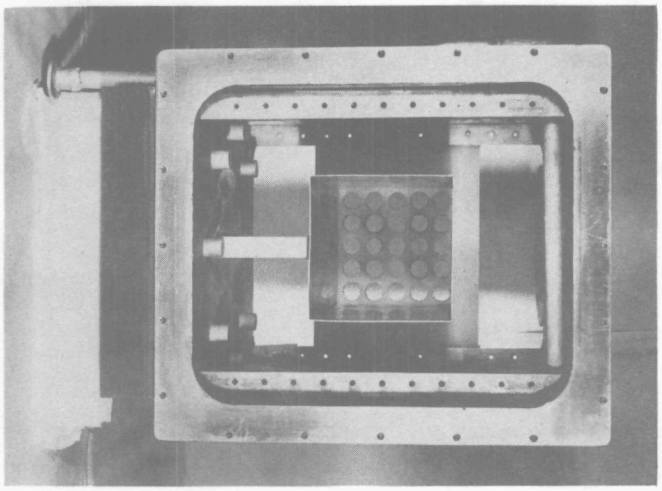

(a)

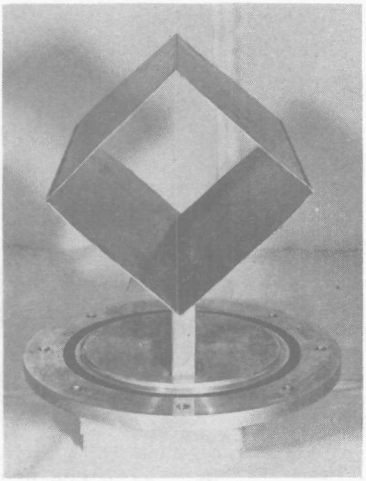

(b)

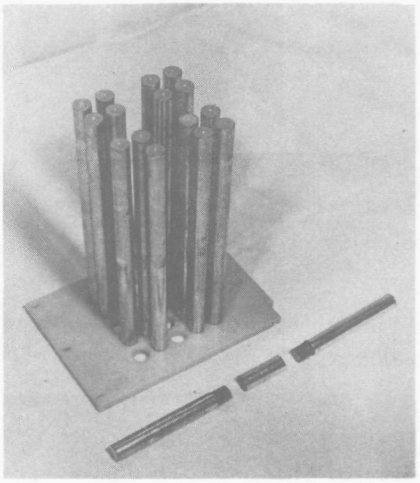

(c)

Fig. 4.10 Experimental set-up for leakage spectrum measurements.
Fig. (a) shows the water container with the side walls removed.
Fig. (b) shows a probe tube for measurements at the corner of the cadmium cylinder.
In Fig. (c) a bundle of iron rods is shown with (in front) an experimental rod for Dy pin measurements.

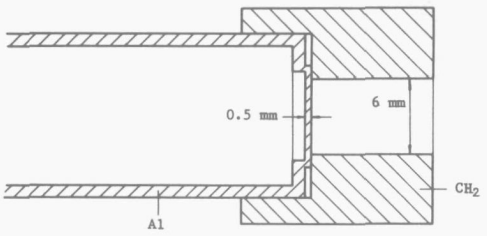

Fig. 4.11 Vertical cross-section of the probe tube with CH_2 frame used for a check on the alignment of the spectrometer.

Below 0.01 eV the counting rate of spectrum neutrons in the measurement was small (lower than 50% of the background counting rate), so that any incorrect background subtraction may also have contributed to the deviation between theory and experiment in the subthermal energy region. Apart from these deviations it may be concluded that THERMOGENE gives a correct prediction of the spectrum in this undermoderated system when linear anisotropic scattering is assumed.

Figs. 4.12 and 4.13 show results obtained from system 7, which is a modification of system 6. A water gap was introduced between four groups of iron rods.

From Fig. 4.12 it may be concluded that reaction rates are predicted correctly within a few per cent in system 7, in which extremely large flux variations are present. The isotropic scattering approximation is clearly still accurate enough. It should be mentioned here that the difference between the results obtained with the two transport models is less than 3.5% with the applied spatial discretization of 143 regions per octant.

Angular spectra were measured in system 7 at 3 positions (Fig.4.13), viz. at the edge (a), at the corner (b) and in the centre (c) of the system. The spectra at positions (a) and (b) were measured with the probe tubes used for system 6; for the measurement of the spectrum at position (c) the bottomless extraction channel used for system 3 was inserted in the water container. The leakage spectrum at position (a) was also measured by filling the extraction channel with a 96 mm long CH_2 platelet. The effect of CH_2 replacing water was thus determined experimentally.

The angular spectrum in the centre of system 7 (position c) was calculated on the assumption of isotropic scattering in order to reduce the

computation problem, as in this case there is only one plane of symmetry in the system. From the results obtained from systems 1, 2 and 3,Fig. 4.3 and Fig. 4.4, it may be concluded that this assumption is no serious source of inaccuracies. The other spectra were calculated with the linear anisotropic scattering approximation.

The agreement between calculation and measurement is pretty good, but there are a few comments to be made:

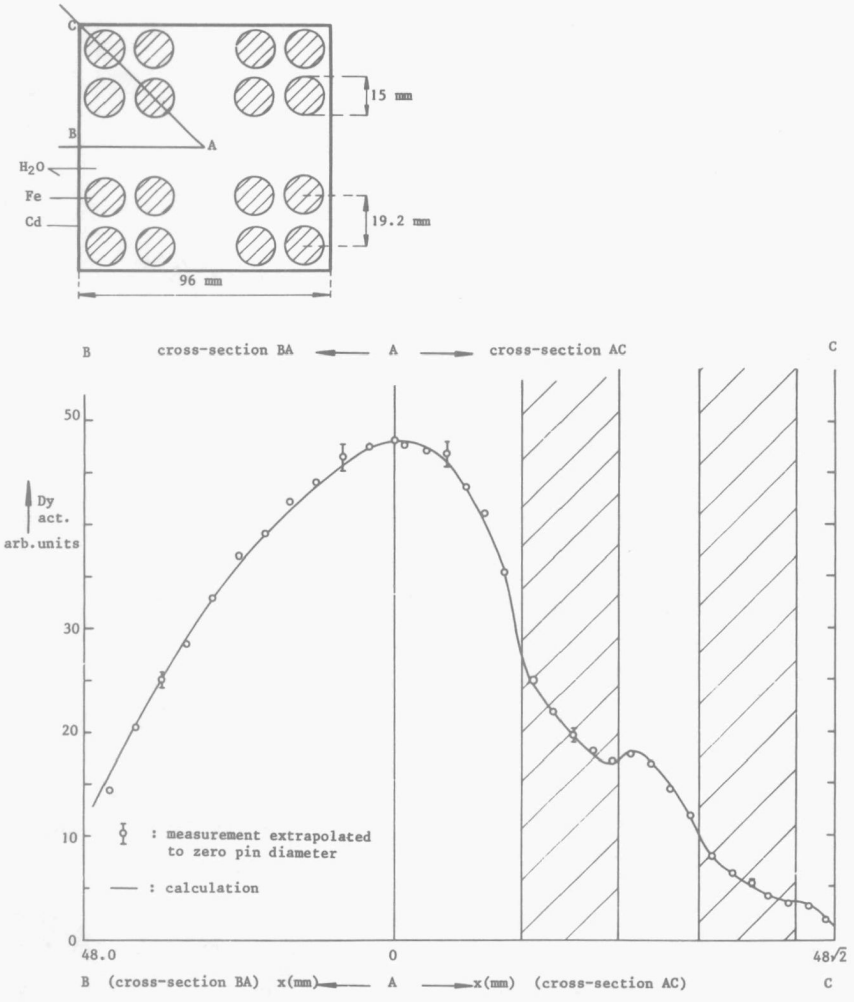

Fig. 4.12 Dy activity in system 7.

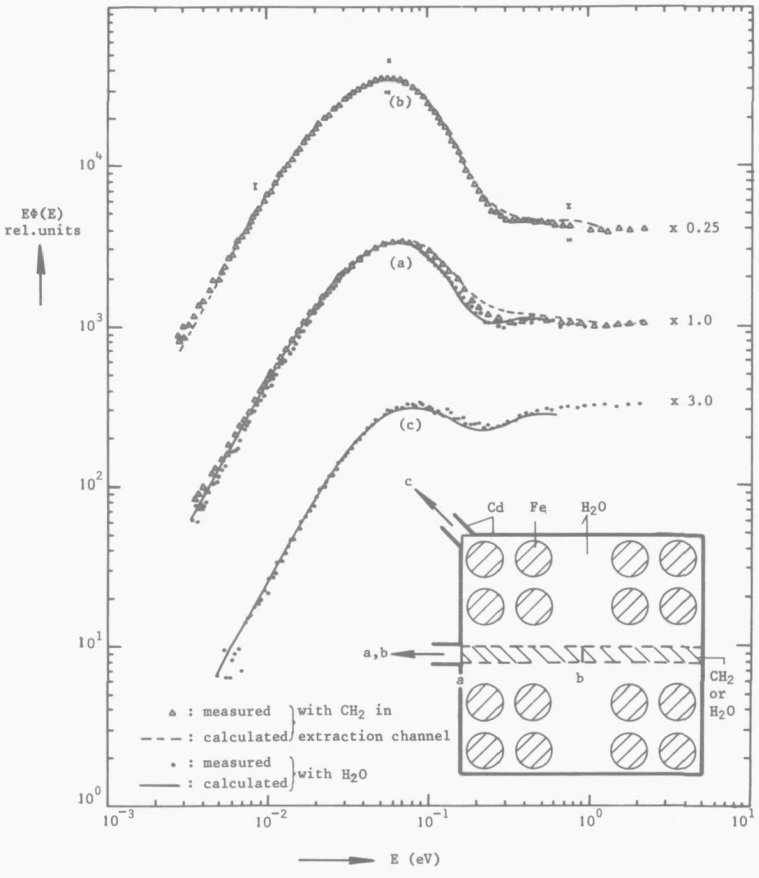

Fig. 4.13 Angular spectra from system 7. Measurements were performed at positions (a) and (c) with the bottomless extraction channel filled with CH_2 (Fig. 4.2), and at positions (a) and (b) with the probe tubes shown in Fig. 4.10.

From the spectra measured at position (a) it can be seen that the deviation between CH_2 and H_2O was underestimated by THERMOGENE for energies below 0.05 eV and overestimated above this energy. Around 0.3 eV a deviation of about 7% between measurement and calculation with CH_2 in the system can be observed. After re-alignment of the spectrometer this spectrum was measured again, but no deviations between the two measured spectra could be observed. It seems justifiable to conclude that the Goldman kernel, in combination with an energy discretization into 21

groups, still needs some improvement. Deviations of a few per cent between theory and experiment in CH_2 slab systems were observed also by Cerbone [19]. The deviation between the calculated and the measured spectrum in the centre of the system (position c) is smaller because this spectrum is fairly well thermalized and anisotropic scattering effects are smaller at this position (cf. the spectrum obtained from system 1, Fig. 4.3).

A slight deviation can be observed between the total flux levels of the spectra, measured and calculated at position (b). Probably the normalization of the measured spectrum with the aid of the monitor system was not sufficiently accurate.

In this section calculations were compared with measurements effected in systems with various flux profiles and spectrum shapes. The Dy activities of experiment and theory agree within the experimental error. The agreement between measured and calculated leakage spectra in water systems is good. The slight differences may be partly due to the small neutron spectrum intensity in the measurements,resulting in a rather large influence of any inaccurate background subtraction, especially in the low-energy region. The effect of spatial discretization in the calculations may also have contributed to the deviations. In systems with mixed rectangular and circular geometries the spatial discretization results in regions with all kinds of shape and with different areas. This discretization should be made very cautiously.

The Goldman scattering model for polyethene does not seem to be adequate under the combined conditions of strong absorption and strong leakage.

4.4 SYSTEMS WITH CADMIUM-LINED RODS

In Sect. 4.3 it was shown that THERMOGENE is adequate for correct prediction of spectra in systems with mixed rectangular and circular geometries. In this section systems will be described in which not only the flux variations in space are large, but also the variations with energy; in other words, the neutron spectra in these systems exhibit a resonance structure. The increasing interest in plutonium recycling in light-

water reactors makes an examination of the reliability of THERMOGENE for mixed U-Pu fuel elements interesting.

The resonance material used for this examination was cadmium, because its resonance energy is fairly low, viz. 0.178 eV (the main resonance energy of ^{239}Pu is 0.296 eV). The circular iron rods were cadmium-covered electrolytically by Stokkermans N.V., Leiden (see Fig. 4.14). A drawback of this method is the fact that the thickness of the cadmium lining was not equal for all rods, whilst the thickness also varied over the surface of a rod because of slight irregularities of the iron surface. The thickness varied between 30 μm and 35 μm.

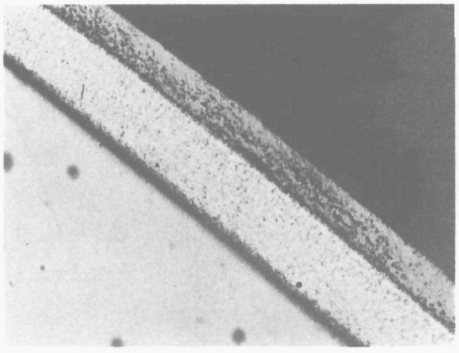

Fig. 4.14 Microscopic view of a cadmium-lined iron rod showing, from left to right, Fe, Cd lining and a Cu coating (which was added for the sake of a better contrast). Magnification ± 300 x. (Photograph by Metallurgical Dept. of Delft Univ. of Techn.)

Fig. 4.15 shows the Dy activity in system 8, which has the same geometry as system 7. Two calculations were effected in which the extreme values of the cadmium thickness were assumed for all the rods. The variation of 15% in the cadmium thickness results in a maximum variation of ∿ 10% in the Dy activity. The measured activity is within the extreme calculated activities. For the spectrum calculations to be described an average thickness of 32 μm has therefore been assumed.

Leakage spectra were measured from system 9 containing 25 cadmium-lined iron rods (see Fig. 4.16). In front of the probe tube those rods were placed which had a lining with a thickness very close to 32 μm (these rods are "seen" by the BF_3 detector). It is evident that the absorption rate in this system was so high that the thermal spectrum disappeared entirely. Comparison between calculation and measurement shows that the theoretical spectrum for subthermal energies is higher than the experimental spectrum. Owing to the very low counting rate in these

measurements the accuracy of the measured data is, however, not high (below 0.01 eV the spectrum counting rate was lower than 10% of the background counting rate). It is, therefore, not possible to decide upon any incorrect prediction of the neutron flux in the subthermal energy region by THERMOGENE (below, this question will be brought up again). The few neutrons in the subthermal energy region give only a minor contribution to the total flux; the deviation between theory and experiment will therefore not be found in the reaction rates, e.g. the Dy activities. Above 0.01 eV the agreement between calculation and measurement is satisfactory except for the energy region around 0.2 eV, where the effect of the finite resolution of the spectrometer to be described below is visible.

In order to establish a more pronounced effect of the resonance in the absorption cross-section of cadmium, leakage spectra were measured

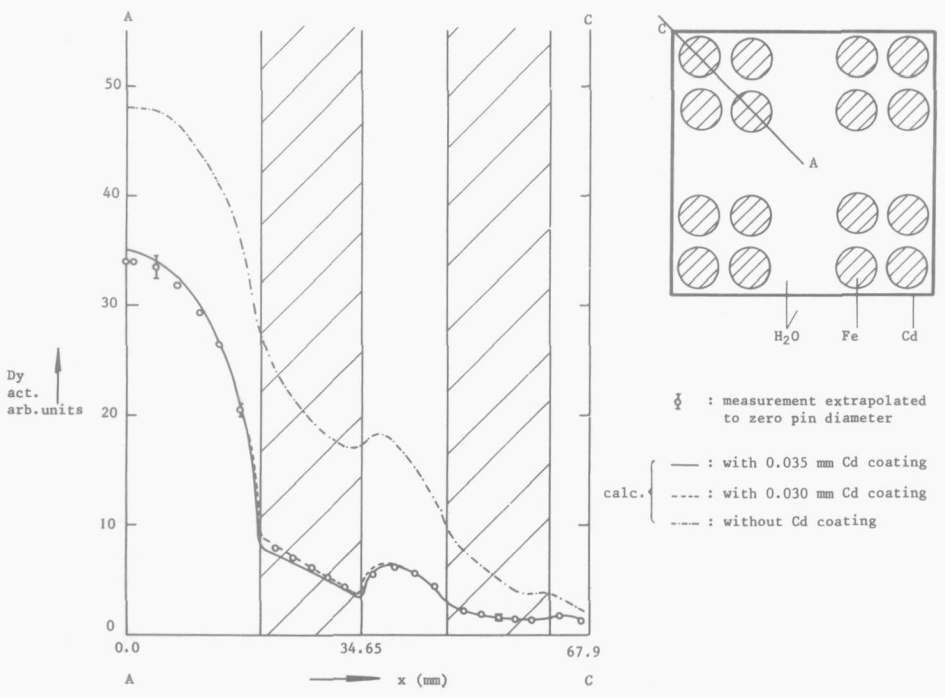

Fig. 4.15 Dy activity in system 8. The iron rods have been coated with a layer of cadmium.

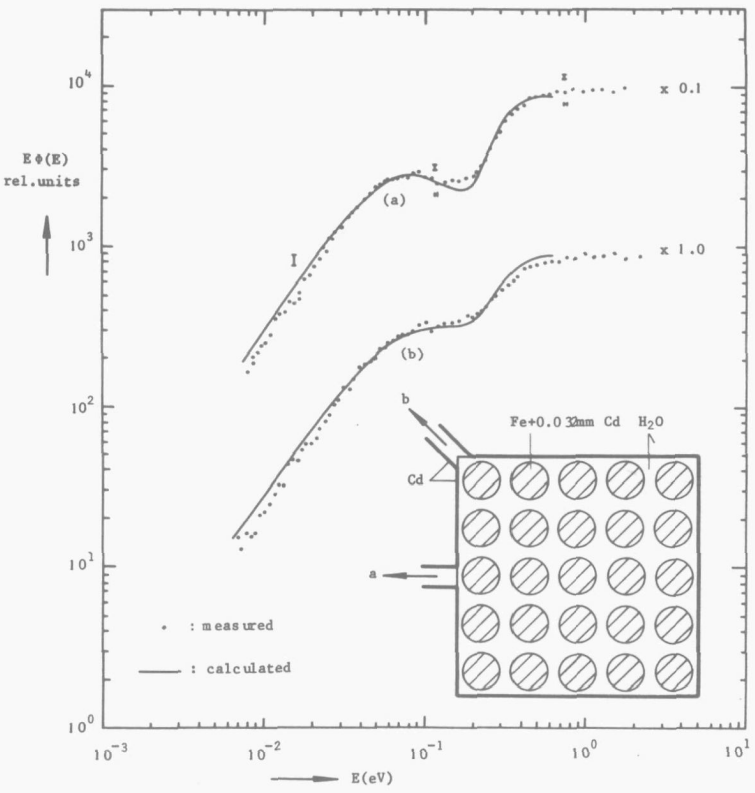

Fig. 4.16 Angular spectra from system 9.

from systems 10 and 11 in which a fairly high thermal flux is present thanks to the small amount of absorbing materials (see Fig. 4.17). Again, one can observe a deviation between measurement and calculation below 0.01 eV. Although the spectrum counting rate was again very low, it seems justifiable to conclude that the calculation model is not sufficiently accurate. The spatial discretization as well as the finite energy discretization could have caused the discrepancies (the cadmium total cross-section is large and changes rapidly with energy). It should, however, be acknowledged that the extreme conditions present in systems 8 to 11 will not be found in any light-water power reactor.

Around 0.2 eV the resonance structure is smoothed somewhat in the measurement owing to the finite resolution of the spectrometer. The

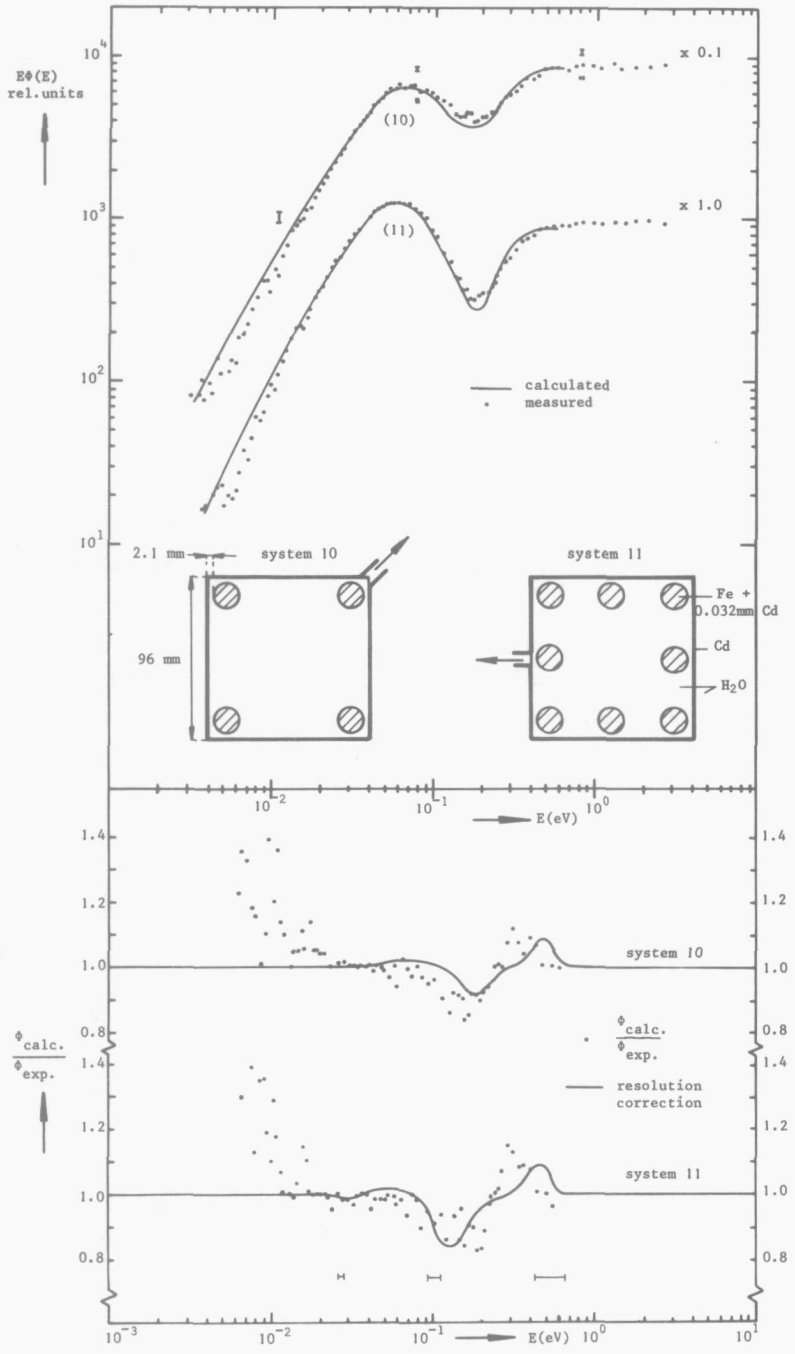

Fig. 4.17 Angular spectra from systems 10 and 11. In the lower part of the figure the deviation between measurement and calculation is compared with the correction to be made in the measured data for the finite resolution of the spectrometer. Here the horizontal bars indicate the energy resolution corresponding to a time resolution of 75 μs.

resolution correction to be made in the measured data was calculated manually, using Eq. (3.3) and a triangular resolution function with a full width at half-height of 75 μs. From the results shown in Fig. 4.17 it can be seen that the deviation between measurement and calculation shows the same trend as the resolution correction. The deviation is slightly greater than the correction, which indicates that the true resolution function is broader than 75 μs. A shift in energy between the deviation and the resolution correction can be observed near 0.45 eV, which may have been caused by incorrect determination of the transmission function of the rotor. As stated in Sect. 3.2.3.3, the transmission function is adapted between 0.15 eV and 0.65 eV to correct for the cadmium lining of the rotor slits which loses its effect for higher neutron energies. It may be that this cadmium correction has not been determined with sufficient accuracy, because the large variation of the flux between 0.15 eV and 0.65 eV in systems 9, 10 and 11 has not been measured before.

In conclusion, it may be stated that the calculated and the measured results for systems with cadmium-lined rods agree within the experimental error. Although each spectrum measurement was continued for about 50 hours, the experimental accuracy for subthermal neutrons was rather poor. A definite conclusion concerning the discrepancy between measurement and calculation for energies below 0.01 eV would require still more accurate measurements.

As regards the calculation model, it may be concluded that THERMOGENE is adequate for predicting thermal neutron spectra in systems with arbitrary complex two-dimensional geometries.

4.5 FINAL REMARKS AND CONCLUSIONS

After the specialized conclusions drawn from the results presented in Sections 4.2, 4.3 and 4.4 it is worth-while to mention some more general conclusions in regard to the experimental and theoretical methods applied in this work.

The adaptation of the spectrometer for high-accuracy measurements in two-dimensional systems and its recalibration required considerable

effort. The reliability of the spectrum measurements was quite satisfactory. All the spectra obtained from systems 6, 7 and 9 were measured twice. Except for system 9a, where the alignment of the spectrometer was not correct during the first run, all the spectra agreed within the statistical accuracy.

The chopper time-of-flight technique shows the disadvantage that only a minor part of the continuous neutron beam from the reactor is used for the spectrum measurements. In the course of the present research this proved to be a serious drawback; the measurements took 10 to 50 hours in order to arrive at a satisfactory statistical accuracy, whilst the radiation level of the irradiated systems was such that the continuation of the experimental program was frequently delayed. A powerful pulsed neutron source such as a LINAC would certainly facilitate the experimental work.

As regards the activation techniques, the method of pin measurements turned out to be an improvement in respect to foil measurements for the determination of flux distributions and peaking factors. A high accuracy could be achieved by conscientious evaluation of the perturbations inherent in the measuring technique.

The THERMOGENE computer program proved to be a powerful means for the prediction of neutron spectra in two-dimensional systems. Two features of the program, viz. application of transport theory (including anisotropic scattering) and exact description of the geometry, constitute a considerable advantage in regard to diffusion or S_N calculations. It should be noted, however, that THERMOGENE is not suitable for complete burn-up studies. The calculation time for the systems described in this chapter was generally about 30 minutes for the IBM 360/65 computer. The incorporation of the program in a modular system for reactor calculations is, however, quite useful, as in this way less accurate (but faster) calculations can be checked against THERMOGENE results. As computers are getting faster the drawback of the long calculation time of THERMOGENE will in future be minimized. Recently some new computing methods, based on integral transport theory, have been published [9, 41, 42, 43, 53, 54]. One might say that integral transport theory is being used more and more for accurate prediction of neutron spectra in two-dimensional systems.

In this thesis the method of solution of the transport equation and the approximations applied in this solution (i.e. discretization of space and energy, isotropic or linear anisotropic scattering) have been tested against experiments. For this reason materials with well-known cross-sections were selected. Considering possible future work, it may be worth-while to compare calculations with measurements in real reactor systems. Spectrum measurements in uniform lattices, effected by Preskitt et al. [44, 45], show satisfactory agreement with theory for uranium lattices, whereas plutonium lattices show deviations which may have been caused by the use of inaccurate cross-sections in the calculations.

As already mentioned, chopped beam time-of-flight measurements cause high radiation levels which are certainly an obstacle to the use of uranium or plutonium in the thermal column of the HOR. The Flash Tube, a pulsed neutron source, which has been constructed by the Delft Reactor Physics Group, may be a useful alternative to the combination of thermal column and chopper, the more so as the resolution of the spectrometer above 0.15 eV is quite low for accurate measurement of the plutonium resonances. Moreover, the experimental system is more accessible if a pulsed neutron source is used, which would facilitate experiments at elevated temperatures and/or with voids in the moderator.

REFERENCES

1. "Fuel Burn-Up Predictions in Thermal Reactors", Proceedings of a Panel, April 1967, IAEA, Vienna (1968).
2. P.G. Aline et al., "Proceedings of a Conference on The Physics Problems in Thermal Reactor Design", Paper 27, BNES, London (1967).
3. H.C. Honeck, "Proceedings of a Symposium on Neutron Thermalization and Reactor Spectra", Paper SM-96/101, IAEA, Vienna (1968).
4. I. Carlvik, "Proceedings of the Third U.N. Int. Conf. on the Peaceful Uses of Atomic Energy", P/681, Geneva (1965).
5. A. Jonsson and H. Pekarek, "Proceedings of The National Topical Meeting of the ANS on Reactor Physics in the Resonance and Thermal Regions", Vol.I, p. 367, The MIT Press, Cambridge (1966).
6. * L.M. Caspers and A.J. Janssen, "THERMOSQUARE, an Algol program for calculating space-dependent neutron spectra in x-y geometries", THD-H-RF 113, Delft (1968).
7. * L.M. Caspers and A.J. Janssen, "PPIXY, a code for calculating probe-tube perturbations with integral x-y transport theory", THD-H-RF 110, Delft (1967).
8. L.M. Caspers, *Comparison between measured and calculated stationary thermal neutron spectra in heterogeneous systems*, Thesis, Delft (1968).
9. R.L. Crowther, "Lectures on Control of Power Reactors", Third International Advanced Summer School in Reactor Physics, IAEA, Vienna (1970), to be published.
10. R.J.J. Stamm'ler, *Fast methods for Computing Thermal Group Constants in single-Pin Lattice Cells*, Thesis, Delft (1968).
11. L.M. Caspers and A.J. Janssen, "Proceedings of a Symposium on Neutron Thermalization and Reactor Spectra", Paper SM-96/44, IAEA, Vienna (1968).

12. H.C. Honeck, "Light Water Lattices", Report of a Panel, 1962, IAEA, Vienna (1962) 233.

13.* A.J. Janssen and G.J. Duin, "THERMOGENE I, a code for calculating thermal neutron spectra in two-dimensional systems with integral transport theory", THD-H-RF 131, Delft (1971).

14.* A.J. Janssen, "THERMOGENE II, a code for calculating thermal neutron spectra in two-dimensional systems with anisotropic scattering", THD-H-RF 135, Delft (1971).

15.* F. Rienstra, "The SCAM code, an Algol code for the calculation of neutron-scattering kernels of hydrogenous moderators",THD-H-RF 103, Delft (1965).

16. J.U. Koppel and J.A. Young, Nucl. Sci. and Eng., 19 (1964) 412.

17. H. Nelkin, Phys. Rev., 119 (1960) 741.

18. D.T. Goldman and F.D. Federighi, Nucl. Sci. and Eng., 16 (1963) 165.

19. R.J. Cerbone et al., Nucl. Sci. and Eng., 30 (1967) 75.

20. D. Newmarch, "Errors due to the cylindrical cell approximation in lattice calculations", AEEW-R34, Winfrith (1960).

21. H.C. Honeck, Trans. Am. Nucl. Soc., 5 (1962) 350.

22. I. Carlvik, "Integral transport theory in one-dimensional geometries", Nukleonik, 10 (1967) 104.

23. I. Carlvik, "Calculations of neutron flux distributions by means of integral transport methods", AE-279, AB Atomenergi, Stockholm (1967).

24. R.G. Harper, "The collision probability code MINOS", J. of Nucl. Energy, 21 (1967) 767.

25. Å. Ahlin, "Instructions for the use of the CLUCOP programme", RFN-202, AB Atomenergi, Stockholm (1965).

26.* A.J. Janssen and R. de Jong, "The DIT-DELFT Programme", THD-H-RF 130, Delft (1970).

27. T.B. Fowler, M.L. Tobias and D.R. Vondy, "EXTERMINATOR-2: a FORTRAN IV code for solving multigroup neutron diffusion equations in two dimensions", ORNL-4078, Oak Ridge (1967).

28. R.J.J. Stamm'ler, "SFINX, multigroup S_4 calculations in x-y geometry", to be published.

29.* K.T. Westerduin, "Koelsysteem voor clusterbak", THD-H-RF 134, Delft (1969).

30.* J.M. van Doorninck and G. van der Pol, "OWL-II, een Algol code voor de omrekening van de met een looptijdspectrometer verkregen waarnemingen tot neutronspectra", THD-H-RF 111, Delft (1967).

31. K.E. Larsson et al., Arkiv för Fysik, 16 (1959) 199.

32. M. Marseguerra and G. Pauli, Nucl. Instr. Meth., 4 (1959) 140.

33. R. de Jong, Afstudeerverslag, THD, Delft (1970).

34.* L.M. Caspers, G.J. Duin and A.J. Janssen, "THERMOSLAB III, an integral transport program for linear anisotropic scattering", THD-H-RF 118, Delft (1968).

35. P.A. Egelstaff and M.J. Poole, *Experimental neutron thermalisation*, Pergamon Press, Oxford (1969).

36. H.C. Honeck, Nucl. Sci. and Eng., 18 (1964) 49.

37. Hiroshi Takahashi, Nucl. Sci. and Eng., 24 (1966) 60.

38. A. Tas and M. Bustraan, "Proceedings of a Symposium on Exponential and Critical Experiments", Paper SM-42/59, IAEA, Vienna (1964).

39. R.J.J. Stamm'ler, S.M. Takač and Z.J. Weiss, "Neutron thermalization in reactor lattice cells: An NPY-Project Report", Technical Reports Series No. 68, IAEA, Vienna (1966).

40. P. Brand, Kandidaatsverslag THD, Delft (1970).

41. Keiichiro Tsuchihashi, "CLUP77: A FORTRAN program of Collision Probabilities for Square Clustered Assembly", JAERI 1196, JAERI (1970).

42. A. Leonard and C.T. Mc Daniel, Trans. Am. Nucl. Soc., 12 (1969) 556.

43. H.S. Cheng, "Integral Transport Theory Methods for Analysis of Control Absorber", to be published.

44. G.D. Trimble et al., "Lattice physics studies, Quarterly progress report for the period ending December 31, 1967", GA-4862, San Diego (1968).

45. G.D. Trimble et al., "Lattice physics studies, Final report", Vol.I, GA-9658, San Diego (1969).

46. J.J. Volpe, "Proceedings of a Symposium on Neutron Thermalization and Reactor Spectra", Paper SM-96/93, IAEA, Vienna (1968).

47. J.G. Carver and C.R. Porter, "Proceedings of a Symposium on Neutron Thermalization and Reactor Spectra", Paper SM-96/61, IAEA, Vienna (1968).

48. G.S. Stanford, "Proceedings of a Symposium on Neutron Thermalization and Reactor Spectra", Paper SM-96/57, IAEA, Vienna (1968).

49. H. Ibarra and R. Sher, Nucl. Sci. and Eng., 29 (1967) 15.

50. J.J. Volpe, J. Hardy Jr. and D. Klein, Nucl. Sci. and Eng., 40 (1970) 116.

51. J.G. Carver et al., Nucl. Sci. and Eng., 41 (1970) 209.

52. A. Gibello et al., Nucl. Sci. and Eng., 40 (1970) 51.

53. A. Leonard and G.T. McDaniel, Trans. Am. Nucl. Soc., 14, no. 1 (1971) 222.

54. H.C. Honeck, Trans. Am. Nucl. Soc., 14, no. 1 (1971) 224.

55. H.C. Honeck, "THERMOS, A thermalization transport theory code for reactor lattice calculations", BNL-5826, BNL (1961).

56. B.G. Carlson, "Solution of the transport equation by S_N approximations", LA-1891, LASL (1955).

*The THD-reports mentioned in this reference list can be obtained from the Reactor Physics Group, Interuniversity Reactor Institute, Delft, The Netherlands.

L I S T O F S Y M B O L S

b	neutron background
B^2	buckling of the neutron flux [cm^{-2}]
D	diffusion coefficient [cm]
E	neutron energy [eV]
E_c	upper limit of thermal neutron energy region [eV]
F	flux peaking factor
H	neutron birth rate density [$cm^{-3}s^{-1}$]
i (index)	region number
J	neutron current [$cm^{-2}s^{-1}$]
k (index)	group number
Ko	total number of energy groups
l_f	neutron flight path [cm]
ℓ (index)	Legendre component
m (index)	Legendre component
M/A	moderator/absorber volume ratio
n	number of spectrum counts in core memory location
n (index)	region number
n_r	rotor velocity [s^{-1}]
No	total number of regions
N_m	monitor normalization factor
r	rotor radius [cm]
r	space co-ordinate [cm]
$\underline{r}$	space vector
r(t)	resolution function of spectrometer [s^{-1}]
R	curvature of rotor slits [cm]
s	width of rotor slits [cm]
s	space co-ordinate [cm]
S	neutron source [$cm^{-3}s^{-1}$]
SI	spectrum index defined by Eq. (3.4)
t	neutron flight time [s]

T	transport kernel [cm]
T	transmission function of rotor
v	neutron velocity [cm s^{-1}]
V	region area [cm^2]
w	number of counts in core memory location
δ	dead time [μs]
Δt_{ch}	time analyser channel width (μs)
ε	detector efficiency
θ	angle indicating neutron flight direction in laboratory system
λ	number of neutron mean free paths
Σ^a	macroscopic absorption cross-section [cm^{-1}]
Σ^s	macroscopic scattering cross-section [cm^{-1}]
Σ^t	macroscopic scattering + absorption cross-section [cm^{-1}]
ϕ	angle indicating neutron flight direction in laboratory system
Φ	neutron flux density [$cm^{-2}s^{-1}$]
$\Phi(E)$	neutron flux per unit energy [$cm^{-2}s^{-1}eV^{-1}$]
$\Phi(\underline{\Omega})$	neutron flux per unit solid angle about $\underline{\Omega}$ [$cm^{-2}s^{-1}$]
$\underline{\Omega}$	neutron flight direction

L I S T O F A B B R E V I A T I O N S

AEEW	Atomic Energy Establishment Winfrith
BNES	British Nuclear Energy Society
BNL	Brookhaven National Laboratory
BWR	Boiling Water Reactor
GA	(Gulf) General Atomic
HOR	Hoger Onderwijs Reactor
IAEA	International Atomic Energy Agency
JAERI	Japan Atomic Energy Research Institute
LASL	Los Alamos Scientific Laboratory
MIT	Massachusetts Institute of Technology
ORNL	Oak Ridge National Laboratory
PWR	Pressurised Water Reactor
THD	Technische Hogeschool Delft (Delft University of Technology)
TOF	Time-of-flight

S U M M A R Y

The purpose of the study described in this thesis has been to develop and test experimentally a computation method for producing thermal neutron energy spectra in non-uniform reactor lattices. Water gaps between bundles of fuel rods (in which cruciform control blades may be present) are examples of irregularities in a lattice. Owing to such irregularities the lattice has to be considered as a two- dimensional system.

In Chapter 1 some comments are made on the consequences of the geometrical complexity for accurate prediction of local peaking factors, conversion factors, reactivity coefficients etc.

A computer program, called THERMOGENE, has been developed for accurate calculation of the space and energy dependent neutron flux in non-uniform lattices. The program has the following features:

(a) It is based on transport theory;

(b) The geometry of a two-dimensional system is taken into account exactly;

(c) The anisotropy of the neutron scattering can be accounted for.

In Chapter 2 the method for solving the transport equation is described, followed by an outline of the principles on which the description of the geometry of a non-uniform lattice is based.

The complexity of both the geometry and the neutron cross-sections of reactor materials necessitates the use of numerical approximations when the transport equation is solved. It is thus necessary to test the accuracy with which neutron spectra are predicted. Therefore, results obtained with THERMOGENE are compared with results of other calculation models. A method to evaluate the effect of spatial discretization is also described in Chapter 2.

Not only the numerical approximations can cause inaccurate results,

but also the used nuclear constants (neutron cross-sections). Verification of the predicted spectra by comparison with "reality", i.e. with experiments, is thus imperative. Chapter 3 deals with the measuring techniques used for this experimental verification. Special attention is paid to the problems arising when measurements have to be carried out with a high degree of accuracy. Two experimental methods have been applied, viz. space-dependent spectrum measurements with a time-of-flight spectrometer, and the activation of lutetium and dysprosium foils or pins, which can be inserted in the lattices.

In Chapter 4 calculations are compared with a series of measurements in systems which were selected in such a way that a large variety of neutron spectra was obtained. Special attention is paid to systems in which a high flux peaking occurred because of the presence of water gaps, systems with a large neutron leakage caused by absorber blades, and systems containing a material which absorption cross-section exhibits a resonance. In this experimental verification light water was used as moderator and uranium was simulated by iron. In some spectrum measurements water was simulated by polyethene in order to simplify the experimental technique.

The results of this investigation can be summarized as follows:

(a) Scalar quantities, e.g. reaction rates, calculated with THERMOGENE, are rather sensitive to the spatial discretization. When the effect of this discretization is accounted for by the method described in Chapter 2, space-dependent reaction rates and local peaking factors are predicted with an accuracy of about 2%. Angular quantities, e.g. the neutron leakage into a control absorber, are less sensitive to the spatial discretization.

(b) Scalar quantities are less sensitive to the effect of anisotropic scattering, compared with angular quantities. A calculation based upon the isotropic scattering approximation will generally suffice. When large flux gradients occur, e.g. near control absorbers, anisotropic scattering should be taken into account in order to calculate the complete angular spectrum with an accuracy of better than 3%.

(c) The Koppel-Young scattering model for light water gives an accurate prediction of the thermalization process in the systems described

in Chapter 4. When the thermal energy region below 0.63 eV is discretized into 10 groups, predicted spectra agree with measured spectra within the experimental accuracy of about 5%, even when the spectra show a resonance structure.

The Goldman scattering model for polyethene does not seem to be accurate enough: a discrepancy of about 7% between theory and experiment near 0.3 eV was observed at locations where a large neutron leakage occurs. Fortunately polyethene is not found in power reactors; it was only used in order to reduce experimental problems.

(d) For some spectra a discrepancy between theory and experiment was observed for neutron energies below 0.01 eV. This occurred in systems with a very low thermal neutron flux owing to a large amount of absorbing materials. Unfortunately, the accuracy of the spectrum measurements in these systems was rather poor, so that no definite conclusion can be drawn whether THERMOGENE correctly predicted the spectra in these rather unrealistic systems or not, although the space- and energy discretization might have been too coarse.

S A M E N V A T T I N G

Het doel van het onderzoek beschreven in dit proefschrift is het ontwikkelen en het, met behulp van metingen, testen van een berekeningsmethode voor de bepaling van thermische neutronenspectra in onregelmatige staafroosters in vermogensreactoren. De onregelmatigheid van de roosters manifesteert zich b.v. in waterspleten tussen bundels splijtstofstaven waarin kruisvormige regelstaven aanwezig kunnen zijn. Door dergelijke onregelmatigheden zal het rooster als een twee-dimensionaal systeem opgevat moeten worden.

In hoofdstuk 1 wordt uiteengezet tot welke complicaties dit leidt voor een nauwkeurige bepaling van plaatselijke piekfactoren, conversiefactoren, reactiviteitscoëfficiënten enz.

Om een nauwkeurige voorspelling te kunnen doen van het plaatsafhankelijke neutronenspectrum is een rekenprogramma ontwikkeld dat:
(a) gebaseerd is op transport theorie;
(b) de geometrie van twee-dimensionale systemen exact kan beschrijven;
(c) de anisotropie van de neutronenverstrooiing in rekening kan brengen.

In het tweede hoofdstuk wordt aangegeven op welke wijze het rekenprogramma, genaamd THERMOGENE, de transportvergelijking oplost en hoe de geometrie van een onregelmatig rooster wordt beschreven.

De gecompliceerdheid zowel van de geometrie als van de neutronen werkzame doorsneden van reactormaterialen maakt het noodzakelijk de transportvergelijking numeriek op te lossen, hetgeen uiteraard tot benaderde uitkomsten leidt. Het is derhalve noodzakelijk THERMOGENE te testen op zijn nauwkeurigheid. Enige rekenresultaten van THERMOGENE worden hiervoor vergeleken met de resultaten van andere berekeningsmodellen. Tevens wordt in hoofdstuk 2 een methode aangegeven waarop de invloed van de plaatsdiscretisatie kan worden bepaald.

Omdat onnauwkeurige resultaten niet alleen kunnen ontstaan door

numerieke benaderingen maar ook door het gebruik van onnauwkeurig bekende nucleaire constanten (werkzame doorsneden), is het noodzakelijk dat de berekende grootheden ook geverifiëerd worden door middel van vergelijking met experimenteel bepaalde grootheden. In hoofdstuk 3 worden de meettechnieken beschreven, welke zijn toegepast voor deze experimentele verificatie, waarbij vooral aandacht wordt besteed aan de wijze waarop met deze technieken metingen kunnen worden gedaan met een hoge graad van nauwkeurigheid. Twee principieel verschillende meetmethoden zijn toegepast, nl. plaatsafhankelijke spectrum metingen met een looptijdspectrometer, en meting van de activiteit van lutetium en dysprosium welke materialen in de vorm van folies of pennetjes in de roosters geplaatst kunnen worden.

In hoofdstuk 4 worden berekeningen met THERMOGENE vergeleken met metingen aan systemen welke zodanig gekozen zijn dat een grote variëteit van neutronenspectra werd verkregen. Hierbij is o.a. gelet op de sterke opslingering van de flux in een waterspleet, de sterke neutronenlek bij absorptieplaten en de grote variatie van de flux als functie van de energie als gevolg van de aanwezigheid van materiaal met een resonantie in de absorptie-werkzame doorsnede. Bij deze verificatie werd licht water als moderator gebruikt terwijl uranium werd gesimuleerd door ijzer. Bij enkele spectrum metingen werd water gesimuleerd door polyetheen ter vereenvoudiging van de meettechniek.

Als voornaamste resultaten van het onderzoek kunnen worden vermeld:

(a) Scalaire grootheden (zoals reactiesnelheden), berekend met THERMOGENE, zijn vrij gevoelig voor de plaatsdiscretisatie. Wanneer de invloed hiervan in rekening wordt gebracht op de in hoofdstuk 2 beschreven wijze kunnen plaatsafhankelijke reactiesnelheden en plaatselijke piekfactoren met een nauwkeurigheid van ca. 2% worden voorspeld. Hoekafhankelijke (vectoriële) grootheden, zoals de lek van neutronen in een regelstaaf, zijn minder gevoelig voor de plaatsdiscretisatie.

(b) Scalaire grootheden zijn minder gevoelig voor het al of niet in rekening brengen van de anisotropie van de neutronenverstrooiing dan vectoriële grootheden. Slechts op plaatsen waar een zeer grote flux gradiënt aanwezig is, zoals in de buurt van regelstaven, kan niet worden volstaan met een isotroop verstrooiingsmodel om het hoekafhankelijke neutronenspectrum met een nauwkeurigheid van beter dan

3% te voorspellen.

(c) Het Koppel-Young verstrooiingsmodel voor water geeft een goede beschrijving van het thermalisatieproces in de onderzochte systemen. De toegepaste energiediscretisatie (10 groepen tussen 0 eV en 0.63 eV) levert resultaten welke, ook voor de spectra waarin resonantiestructuur aanwezig is, overeenstemmen met de gemeten spectra binnen de meetnauwkeurigheid van ca. 5%.
Het Goldman verstrooiingsmodel voor polyetheen veroorzaakt een afwijking tussen theorie en experiment bij 0.3 eV van ca. 7% op plaatsen waar een grote neutronenlek optreedt. Voor polyetheen is een beter verstrooiingsmodel aan te bevelen.Hierbij moet echter worden opgemerkt dat polyetheen slechts gebruikt is uit experimenteel-technische overwegingen en in vermogensreactoren niet voorkomt.

(d) Bij spectra in systemen met een zeer lage thermische flux tengevolge van de aanwezigheid van veel absorberend materiaal treedt een afwijking op tussen theorie en experiment voor neutronenenergieën beneden 0.01 eV. De nauwkeurigheid van de metingen was hier echter zo laag dat geen definitieve conclusie mogelijk is over een al dan niet juiste voorspelling van het spectrum door THERMOGENE, ofschoon de plaats- en de energiediscretisatie hier mogelijk te onnauwkeurig zijn geweest.

A C K N O W L E D G E M E N T S

The subject of this investigation has been suggested by Dr. L.M. Caspers. The author is indebted to him and to other members of the Reactor Physics Group for valuable discussions.

Considerable help in the development and programming of the computer program THERMOGENE was given by G.J. Duin. His contribution is gratefully acknowledged.

Thanks are due to P. Brand, R. de Jong and D.J. van den Hoek, who participated as students in various parts of this study while fulfilling the requirements for the degree of Natuurkundig Ingenieur.

The author feels indebted to W.P. van den Broek, K.M. Dijkman, K.N. Eindhoven, C.A. Rieff, K.J. Roos and K.T. Westerduin for skillfull assistance in the performance of the measurements.

The author would like to thank the members of the Reactor Division and the Health Physics Division of the Interuniversity Reactor Institute for their pleasant co-operation and Miss Linda Dornseiffer for typing the manuscript.